# Simplified analytical model for sound level prediction at shielded urban locations involving multiple diffraction and reflections

Weigang Wei, Timothy Van Renterghem[a)], and Dick Botteldooren

Ghent University

Department of Information Technology

Sint-Pietersnieuwstraat 41, B-9000 Ghent, Belgium

[a)]e-mail: timothy.van.renterghem@intec.ugent.be

**Abstract**

Accurate and efficient prediction of the sound field in shadow zones behind obstacles is a challenging task, but essential to produce urban noise maps. A simplified method is presented to predict sound levels at shielded urban locations, including multi-edge diffraction over successive buildings and multiple reflections between parallel façades. The model is essentially based on Pierce's diffraction theory, where the Fresnel Integral is approximated by trigonometric functions for efficient evaluation, and parameterized for urban environments. The model has been validated for idealized urban configurations by comparing to the results of Pierce's theory and a full-wave numerical method. In case of multi-edge diffraction over buildings in absence of a source or receiver canyon, deviations from the full-wave simulations are smaller than 2 dB for the octave bands with central frequencies ranging from 125 to 1000 Hz. However, larger errors are made when receivers are close to the extension line from the diffraction edge closest to the receiver. In case of combining the simplified multi-edge diffraction model with an efficient approach for including the series of mirror sources and mirror receivers, based on the Hurwitz-Lerch transcendent, this same accuracy is obtained.

## I. INTRODUCTION

Predicting sound pressure levels at highly shielded areas, e.g. in the deep shadow zone of a conventional noise wall or at non-directly exposed façades and in courtyards in an urban setting, is a challenging sound propagation problem. Many researchers developed analytical, semi-analytical and empirical calculation strategies for sound diffracting over thin screens, thick screens and multi-edge objects[1;2;3;4;5;6;7;8]. An explicit solution, aiming at solving the diffraction of line sources, can also be found in literature[9;10]. In general, such models are able to predict the diffracted sound fields well. The reader is referred to some review articles[11;12] for a detailed analysis of previously proposed models and scale model studies[13;14]. For application to urban noise maps, however, not only accuracy but also calculation speed is a major issue, making many of these previously cited approaches not well suited for this specific task. At the other hand, models allowing a fast evaluation are unable to predict sound pressure levels with a sufficient accuracy at highly shielded urban locations like e.g. the screening formula used in the ISO9613-2 model.

The diffraction formula used in this study is essentially based on Pierce's diffraction theory[3], where the Fresnel Integral is approached by trigonometric functions for efficient evaluation, and parameterized for typical urban environments as discussed by Wei et al.[15]. The model has been further evaluated in this paper for general multi-edge diffraction problems.

In an urban environment, not only diffraction but also accounting for the multiple reflections in between opposing building façades could strongly increase the computational burden. As a consequence, the number of reflections (and associated number of mirror sources and mirror receivers) is limited in most noise mapping efforts. However, this results in significant loss of accuracy. Previously, Heutschi[16] proposed look-up tables to predict urban street sound pressure levels based on source-receiver positioning and street geometry, while Thomas et al.[17] proposed to add the energy present in the reverberant part of the sound field based on regression analysis of a large dataset of measurements in urban streets. In this paper, the reverberant field approach that underlies these developments, is extended to propagation towards a shielded area. Theoretical analysis of the mirror source series contributing to a shielded receiver is efficiently approached by parameterization.

The paper is organized as follows. After the Introduction, the simplified diffraction formulas as previously presented in Wei et al.[15] are summarized in Sections II. A and II. B, providing additional validation and analysis of CPU time. In Section II. C, this diffraction approach is generalized to multiple edge diffraction. In Section III, a method is proposed to include the effect of multiple reflections for sound propagation towards shielded urban locations. Finally, a Discussion (Section IV) and Conclusion (Section V) are provided.

## II. A SIMPLIFIED METHOD TO CALCULATE DIFFRACTION

To avoid confusion, some frequently used nomenclature is listed below:

- $i$ equals $\sqrt{-1}$, indicating the imaginary part.
- $D$ is the diffraction function.
- $l$ is the number of diffracting edges. For example, $D_l$ indicates the diffraction function at the $l^{th}$ edge.
- $\beta$ is the angle of the diffracting wedge, e.g. $\beta_S$ is the angle of the diffraction edge closest to the source and $\beta_l$ is the angle of the $l^{th}$ diffraction edge.
- $\theta_{s,l}$ is the angle from the right face of the $l^{th}$ diffraction edge to the connecting line from the source to the diffraction edge.
- $\theta_{r,l}$ is the angle from the right face of the $l^{th}$ diffraction edge to the connecting line from the receiver to the diffraction edge.
- $a$ is the number of image sources.
- $b$ is the number of image receivers.
- $r_s$ is the distance from the source to the closest diffraction edge.
- $r_r$ is the distance from the receiver to the closest diffraction edge.
- $r_{s,l}$ is the distance of the propagation path from the source to the $l^{th}$ diffraction edge.

- $r_{r,l}$ is the distance of the propagation path from the $l^{th}$ diffraction edge to the receiver. The receiver can be the real receiver or can be the next diffraction edge.
- $r_{s,a}$ is the distance of the $a^{th}$ image source to the closest diffraction edge.
- $r_{r,b}$ is the distance of the $b^{th}$ image receiver to the closest diffraction edge.
- $\lambda$ is the wave length.
- $W$ is the width of a thick barrier or the width between two diffraction edges.
- $j$ is a local index indicating the change of diffraction edges, for example $W_{j,j+1}$ is the distance from the $j^{th}$ edge to $(j+1)^{th}$ edge.

## A. Single diffraction at a rigid-wedge

According to previous studies[3;5;6;18], the diffracted sound pressure is a product of a source term, a term related to the propagation distance and a diffraction term. For a point source diffracted by a rigid wedge, the diffracted sound pressure then reads:

$$p_{diffr} = S_0 \frac{e^{ikL}}{L} D_1, \tag{1}$$

where $D_1$ is the diffraction function which depends on $\theta_{s,l}$, $\theta_{r,l}$, $r_{s,l}$, $r_{r,l}$ and $\beta_l$. The subscript 1 of $D$ indicates diffraction happening at the $1^{st}$ edge. Clearly, in rigid-wedge

diffraction $l = 1$, meaning there is only one diffraction edge. $L$ is the total length of the propagation path and $S_0$ is the strength of the source. The asymptotic solution of $D$ in Pierce's[3] work seems most interesting to allow further simplification:

$$D_1(r_{s,1}, \theta_{s,1}, r_{r,1}, \theta_{r,1}, \beta) = \frac{e^{i\pi/4}}{\sqrt{2}} \left[A_D(X_+) + A_D(X_-)\right], \tag{2}$$

where $X_+ = \Gamma M_\nu(\theta + \theta_0)$, $X_- = \Gamma M_\nu(\theta - \theta_0)$, $\Gamma = \sqrt{2r_s r_r/[\lambda(r_r + r_s)]}$, $M_\nu(\theta) = \dfrac{\cos\nu\pi - \cos\nu\theta}{\nu \sin\nu\pi}$, $\nu = \pi/\beta$. Clearly, in this case $\theta_{s,1} = \theta_0$ and $\theta_{r,1} = \theta$. The definition of the angles is shown in Fig. 1. Other parameters are:

$$A_D(X) = \frac{\sqrt{2}}{2\pi} \int_{-\infty}^{\infty} \frac{e^{-u}}{X\sqrt{\frac{\pi}{2}} - e^{-i\pi/4}u} du = sign(X) \left[f(|X|) - ig(|X|)\right], \tag{3}$$

$$f(X) = [\frac{1}{2} - S(X)] \cos(\frac{1}{2}\pi X^2) - [\frac{1}{2} - C(X)] \sin(\frac{1}{2}\pi X^2), \tag{4}$$

$$g(X) = [\frac{1}{2} - C(X)] \cos(\frac{1}{2}\pi X^2) + [\frac{1}{2} - S(X)] \sin(\frac{1}{2}\pi X^2), \tag{5}$$

$$C(X) = \int_0^X \cos\left(\frac{1}{2}\pi t^2\right) dt, \tag{6}$$

$$S(X) = \int_0^X \sin\left(\frac{1}{2}\pi t^2\right) dt. \tag{7}$$

Although the Fresnel Integrals can be solved rather easily nowadays, further simplification is still useful. If $X \gg 0$, the Fresnel Integral can be simplified as $C(X) \approx 0.5 + \frac{1}{\pi X}\sin\left(\frac{\pi}{2}X^2\right)$ and $S(X) \approx 0.5 - \frac{1}{\pi X}\cos\left(\frac{\pi}{2}X^2\right)$. However, in real urban cases, $x \to 0$ appears frequently, implying that $S(X) \approx 0.5 - \frac{1}{\pi X}\cos\left(\frac{\pi}{2}X^2\right)$ has a strong singularity point at $X = 0$. The later means that this approximation can lead to big errors when $X$ is close to 0. To avoid this singularity, the Fresnel Integrals are approximated by[15]:

$$C(X) \approx 0.5 + \frac{0.37}{0.37 + X}\sin\left(\frac{\pi}{2}X^2\right), \tag{8}$$

$$S(X) \approx 0.5 - \frac{0.37}{0.37 + X}\cos\left(\frac{\pi}{2}X^2\right). \tag{9}$$

The coefficient 0.37 is found by fitting to the solution of the Fresnel Integrals with typical urban geometrical inputs. The largest approximation error appears when the receiver is on the reflection or shadow boundary, which is indicated by $X \to 0$ in Fig. 2. Figure 3, which is extracted from the urban structure of two European cities (Ghent, in Belgium, and Katendrecht, Rotterdam, in the Netherlands), shows the distribution of $X$-values. Although for a considerable number of cases $X$ is close to zero, most values exceed 1.

Substituting Eq. (8) and (9) into Eq. (4) and (5) leads to:

$$f(X) = \frac{0.37}{X + 0.37}, \tag{10}$$

$$g(X) = 0. \tag{11}$$

Then the diffraction function Eq. (2) of a single rigid-wedge becomes:

$$D_1(r_s, \theta_{s,1}, r_r, \theta_{r,1}) = \frac{e^{i\pi/4}}{\sqrt{2}} \left[ f(X_+) + f(X_-) \right] = \frac{e^{i\pi/4}}{\sqrt{2}} \left( \frac{0.37}{0.37 + X_+} + \frac{0.37}{0.37 + X_-} \right), \tag{12}$$

where the definition of $X_+$, and $X_-$ are the same as in Eq. (2).

Since strict but complicated formulas of single-wedge and double-edge diffraction have been given in Pierce's work, the simplified equations proposed in this work will be compared with Pierce's theoretical solution. Figure 4 shows the amplitude difference, $10 \log_{10} \left| \frac{p_{dif}}{p_{at,L}} \right|^2 = 10 \log_{10} \left( \frac{1}{2} \left\{ [g(X_+ + g(X_-))]^2 + [f(X_+ + f(X_-))]^2 \right\} \right)$, between the diffracted case and free field propagation. The simplified method properly follows Pierce's solution. The ratio between wave lengths and the geometrical dimension of urban buildings may differ from 1 to 100. Therefore, three groups with different wave lengths are compared in Fig. 4.

By using Eqs.(10) and (11), the calculation time is reduced considerably. Figure 5 shows the ratio in CPU evaluation time between Pierce's method and the simplified method in case of a single-wedge and double-edged rigid barrier (see next section). CPU time ratios exceed 10000.

## B. Diffraction function of a double-edge rigid barrier

A double-edge diffraction as shown in Fig. 1 (b) can be expressed as a single diffracted wave produced from edge 1 and then subsequently diffracted by edge 2 to reach the receiver. More details could be found in[5;18]. Then, the corresponding angle of $\theta$ and $\theta_0$ diffracted by the path $S \to 1 \to 2$, are 0 and $\beta_S - \theta_S$, respectively. Accordingly, $X_{S+} = \gamma M_\nu(\theta + \theta_0) = \gamma M_\nu(\beta_S - \theta_S)$ and $X_{S-} = \gamma M_\nu(\theta - \theta_0) = \gamma M_\nu(\theta_S - \beta_S)$. Instead of $\Gamma$, $\gamma = \sqrt{2r_S(W + r_r)/[\lambda(r_S + W + r_r)}$ is used to calculate $X$ in the double-edge diffraction case and $M_\nu$ is the same as in the single rigid-wedge case. Note that $M_\nu(\theta) \propto \cos \nu\theta$ leading to $X_{s+} = X_{S-}$. For the second part of the double-edge diffraction path $1 \to 2 \to R$, $X_{R+} = X_{R-}$.

Based on the above analysis, the diffraction function of a double connected edge then reads:

$$\begin{aligned} D &= D_1(r_{s,1}, \theta_{s,1}, r_{r,1}, \theta_{r,1}, \beta_1) D_2(r_{s,2}, \theta_{s,2}, r_{r,2}, \theta_{r,2}, \beta_2) \\ &= \frac{1}{2}\frac{e^{i\pi/4}}{\sqrt{2}} \left[f(BX_{S+}) + f(BX_{S-})\right] \frac{e^{i\pi/4}}{\sqrt{2}} [f(X_{R+}) + f(X_{R-})] \\ &= i\left(\frac{0.37}{0.37 + BX_{S+}} + \frac{0.37}{0.37 + BX_{S-}}\right)\left(\frac{0.37}{0.37 + X_{R+}} + \frac{0.37}{0.37 + X_{R-}}\right). \end{aligned} \tag{13}$$

As shown in Fig. 2, in a double-edge diffraction, $r_{s,1} = r_s$, $\theta_{s,1} = \beta_S - \theta_s$, $r_{r,1} = W$, $\theta_{r,1} = 0$, $r_{s,2} = r_s + W$, $\theta_{s,2} = \beta_R$, $r_{r,2} = r_r$ and $\theta_{r,2} = \theta_r$. In this case, $\beta_1 = \beta_2 = 1.5\pi$. The

factor 1/2 is used to remove the mirror image on the connecting surface. Because of $X_{S+} = X_{S-}$ and $X_{R+} = X_{R-}$,

$$D = i[f(BX_{S+})f(X_{R+})] = i\left(\frac{0.37}{0.37 + BX_{S+}}\frac{0.37}{0.37 + X_{R+}}\right), \tag{14}$$

where $B = \sqrt{WL/[(W + r_S)(W + r_r)]}$ is a scalar multiplied to the smaller one of $X_{S+}$ and $X_{R+}$[35]. In Eq. 14, $X_{S+} < X_{R+}$ is assumed. This assumption is met in most urban geometries. Details can be found in[15].

Figure 4 (b) compares double-edge diffraction as predicted by Pierce and the simplified method as calculated by Eq. (14) with the parameters $r_s = 10\lambda$, $r_r = 10\lambda$, $W = 10\lambda$, $\theta_s = \pi/4$, $\beta_s = 3/2\pi$, $\beta_r = 3/2\pi$; $\theta_r$ increases from 0 to $\pi/2$. Except for predictions along the extension line of the barrier top, the simplified model results match Pierce's solutions quite well for the chosen parameter set.

### C. Generalization to multiple diffraction

Generalization to multiple diffraction is essential in urban cases where sound typically propagates over subsequent buildings. In Kawai's[5] and Chu's[18] generalization, the double diffraction can be expressed by the product of two single diffraction where the incident wave for the second diffraction comes from the first diffraction edge. Similarly, multiple diffraction can be considered as a series of successive diffractions[18]. The $(n-1)^{th}$ diffracted

sound pressure by path $S1\cdots n$ is:

$$p_{n-1}^{S1\cdots n} = p_{n-2}^{S1\cdots n-1}\frac{L_{n-2}}{L_{n-1}}D_{n-1}e^{ik(L_{n-1}-L_{n-2})}, \tag{15}$$

where $D_n$ is the diffraction function at the $n^{th}$ edge; $L_n$ is the total diffraction path length. In the case presented in Fig. 1, $L_1 = r_s + W_{12}$, $L_2 = r_s + W_{12} + W_{23}$. Other path lengths are similar.

According to Eq. (15), $p_{n-2}^{S1\cdots n-1} = p_{n-3}^{S1\cdots n-2}\frac{L_{n-3}}{L_{n-2}}D_{n-2}e^{ik(L_{n-2}-L_{n-3})}$. Therefore, Eq. (15) becomes:

$$\begin{aligned} p_{n-1}^{S1\cdots n} &= p_{n-3}^{S1\cdots n-2}\frac{L_{n-3}}{L_{n-2}}D_{n-2}e^{ik(L_{n-2}-L_{n-3})}\frac{L_{n-2}}{L_{n-1}}D_{n-1}e^{ik(L_{n-1}-L_{n-2})} \\ &= p_{n-3}^{S1\cdots n-2}\frac{L_{n-3}}{L_{n-1}}D_{n-2}D_{n-1}e^{ik(L_{n-1}-L_{n-3})}. \end{aligned} \tag{16}$$

If the diffracted sound pressure is recursively replaced by Eq. (15), $p_{n-1}^{S1\cdots n}$ becomes:

$$p_{n-1}^{S1\cdots n} = p_1^{S12}\frac{L_1}{L_{n-1}}D_2 ... D_{n-1}e^{ik(L_n-L_1)}. \tag{17}$$

Substituting Eq. (1) in the above, the sound pressure at the $n^{th}$ diffraction point or at a receiver point after n-1 diffractions then reads:

$$p_{n-1}^{S1\cdots n} = \left(\frac{1}{2}\right)^C S_0\frac{e^{ikL_{n-1}}}{L_{n-1}}\prod_{l=1}^{n-1}D_l \qquad n = 2, 3, \cdots . \tag{18}$$

Equation (18), see also Kim[6], is a generalized form of a multiple diffraction function which equals the product of the geometrical divergence and its diffraction function $D_l$:

$$D_l(r_{s,l}, \theta_{s,l}, r_{r,l}, \theta_{r,l}, \beta_l) = \frac{e^{i\pi/4}}{\sqrt{2}}[f(B_l X_{l+}) + f(B_l X_{l-})] = \frac{e^{i\pi/4}}{\sqrt{2}}\left(\frac{0.37}{0.37 + B_l X_{l+}} + \frac{0.37}{0.37 + B_l X_{l-}}\right), \tag{19}$$

with $X_{l+} = \gamma_l M_\nu(\theta_{l+})$, $X_{l-} = \gamma_l M_\nu(\theta_{l-})$, $\theta_{l+} = \theta_{s,l} + \theta_{r,l}$, where $\theta_{r,l}$ the angle from the right diffraction edge and the connecting line between the diffraction edge to the "receiver" and $\theta_{s,l}$ the angle from the right diffraction edge to the connecting line between the diffraction point to the "source". For the definition of these angles, "source" and "receiver" can be the real source and receiver or can be the adjacent diffraction edges. $\theta_{l-} = \theta_{s,l} - \theta_{r,l}$. $\gamma_l$ will be discussed later. $n$ is the diffraction number. $C$ is the number of adjacent double diffraction edges. In series of non-connected building blocks, $C$ equals 1 as the diffraction path $S \to 1 \to 2 \to 3 \to 4 \to$ in Fig. 1 (c). As shown in Fig. 1 (c), the sound pressure at receiver $R$ consist of contributions from different propagation paths. The shortest path with the smallest number of diffractions, $S \to 1 \to 2 \to 3 \to 4 \to R$, will dominate the sound pressure. In this study, only the shortest path is discussed, which implies $C = 1$ in most conditions. A typical case when $C$ is greater than 1 is a single many-edged building, as shown in Fig. 1 (d).

For multiple-diffraction, $B(r_s, r_r, W) = \sqrt{W(r_s + r_r + W)/[(W + r_s)(W + r_r)]}^5$ is

generalized to:

$$\begin{aligned}
B_1 &= B(r_s, W_{23} + W_{34} + \cdots + W_{n-1,n} + r_r, W_{12}),\\
B_2 &= B(r_s + W_{12}, W_{34} + \cdots + W_{n-1,n} + r_r, W_{23}),\\
&\vdots\\
B_l &= B(r_s + W_{12} + \cdots + W_{l-1,l}, W_{l+1,l+2} + \cdots + W_{n-1,n} + r_r, W_{l,l+1}),\\
&\vdots\\
B_{n-1} &= B(r_s + W_{12} + W_{23} + W_{34} + \cdots + W_{n-2,n-1}, r_r, W_{n-1,n}),\\
B_n &= 1,
\end{aligned} \tag{20}$$

resulting in the following closed form:

$$\begin{aligned}
B_l &= \sqrt{\frac{W_{l,l+1}(r_s + \sum_{j=1}^{n-1} W_{j,j+1} + r_r)}{(W_{l,l+1} + r_s + \sum_{j=1}^{l-1} W_{j,j+1})(W_{l,l+1} + r_r + \sum_{j=l+1}^{n-1} W_{j,j+1})}}\\
&= \sqrt{\frac{W_{l,l+1}(r_s + \sum_{j=1}^{n-1} W_{j,j+1} + r_r)}{(r_s + \sum_{j=1}^{l} W_{j,j+1})(r_r + \sum_{j=l}^{n-1} W_{j,j+1})}}.
\end{aligned} \tag{21}$$

$\gamma(r_s, r_r, L) = \sqrt{2r_s r_r/(\lambda L)}$ is generalized to:

$$
\begin{aligned}
\gamma_1 &= \gamma(r_s, W_{12} + W_{23} + W_{34} + \cdots + W_{n-1,n} + r_r, L), \\
\gamma_2 &= \gamma(r_s + W_{12}, W_{23} + W_{34} + \cdots + W_{n-1,n} + r_r, L), \\
&\vdots \\
\gamma_l &= \gamma(r_s + W_{12} + W_{23} + \cdots + W_{l-1,l}, W_{l,l+1} + W_{n-1,n} + r_r, L), \\
&\vdots \\
\gamma_n &= \gamma(r_s + W_{12} + W_{23} + W_{34} + \cdots + W_{n-1,n}, r_r, L),
\end{aligned} \tag{22}
$$

or

$$
\gamma_l = \sqrt{\frac{2\left(r_s + \sum_{j=1}^{l-1} W_{j,j+1}\right)\left(r_r + \sum_{j=l}^{n-1} W_{j,j+1}\right)}{\lambda\left(r_s + \sum_{j=1}^{n-1} W_{j,j+1} + r_r\right)}}, \tag{23}
$$

where $r_s$ is the distance from the source to the first diffraction edge; $W_{l,l+1}$ is the distance between edge $l$ and edge $l+1$; $r_r$ is the distance from the receiver to the last diffraction edge. $M_\nu(\theta) = (\cos\nu\pi - \cos\nu\theta)/(\nu\sin\nu\pi)$ is generalized to

$$
M_{\nu l}(\theta_l) = (\cos\nu_l\pi - \cos\nu_l\theta_l)/(\nu_l\sin\nu_l\pi). \tag{24}
$$

When $n = 3$, Eq. (18) models a double-edge diffraction. Since $X_{l+} = X_{l-}$ in this special case, $\prod D = i\left(\frac{0.37}{0.37 + B_1X_{1+}}\frac{0.37}{0.37 + B_2X_{2+}}\right)$, where

$B_1 = \sqrt{WL/[(W + r_S)(W + r_r)]}$, $B_2 = 1$. $B_1$ will be multiplied to the smaller one of $X_{1+}$ and $X_{2+}$. Here $X_{1+} < X_{2+}$ is assumed.

### D. Validation of the multiple-edge simplified diffraction model

The proposed model is validated for the case of sound propagation over successive buildings, involving multiple edge diffraction. Various cases are presented in Fig. 6, including a high rectangular building in between two lower ones near the source and receiver, a high building directly near the source followed by lower buildings towards the receivers, and a high thin barrier in between two buildings. The last case is not very common in a city, however, it can be used as a good validation case to include a single diffraction as well. Contour plots of the differences between the simplified method and the diffraction formula by Pierce are depicted in Figs. 7 to 10, for 250 Hz and 2000 Hz. In these calculations, the shortest propagation path and only diffraction over the roofs were considered. Note that multiple reflections in between the façades are not considered in neither of these models.

At most receiver positions in the shadow zone of the building furthest away from the source, the predicted values by the simplified method are close to the theoretical values. However, a clear zone with overestimations along the (virtual) extension line of the diffraction boundary is observed. The simplified method can thus be used to predict sound

propagation diffracted by multiple edges within 2 dB at strongly shielded areas. Near the extension line of the diffraction edge, an overestimation of 3 dB is obtained. Note that predicting diffraction in this specific zone is a complicated topic and contradictory to the goal of this work which is rather to simplify models. More theoretical solutions to tackle this problem can be found in literature[1;3].

## III. CONTRIBUTION OF REFLECTIONS

When sources and receivers are located in so-called "city canyons", multiple reflections in both the source and receiver canyon become relevant. The latter is typically solved by considering image (mirror) sources and image receivers[20;21;22]. The position of the image sources and receivers is easily obtained by geometrical analysis of the problem under study.

In Fig. 11, the circles and triangles are image sources and image receivers, respectively. Ground reflections are not considered here. The distance from the image source to the façade increases with the order of reflection. The first image source is at $W_{s1}$ from the left façade of the source canyon. The second image source towards the left side is located at $W_{s2} + W_s$; the third one at $W_{s1} + 2W_s$. When generalizing, this yields :

$$d_a = \begin{cases} W_{s1} + (a-1)W_s & a = 1, 3, 5 \cdots \\ W_{s2} + (a-1)W_s & a = 2, 4, 6 \cdots \end{cases}$$

For simplicity, suppose the source is in the center of the canyon, so $W_{s1} = W_{s2}$.

Consequently, the distance from the image source to the façade is then $aW_s - 0.5W_s$, where $a$ is the $a$th image source.

Considering an insufficient number of mirror sources will strongly underestimate levels. Calculations show that including 50 image source, relative to only considering two, may add at least 4 dB, strongly depending on the assumed reflection coefficient of the façades in the source canyon as shown in Fig. 12 (a). Similar estimates can be found in[23;24]. In Fig. 12 (a), a fixed configuration is used and only the reflection coefficients of the façades are varied. Figure 12 (b) shows the effect of the source canyon width and right-façade building height of the source canyon for a reflection coefficient of 0.97. The underestimation in sound pressure level by only considering the $1^{st}$ image source ranges from 5 dB to 13 dB.

Increasing the number of image sources increases the computing time considerably. As a result, only one or two image sources are typically considered in urban noise mapping. However, the simplified form as shown in Eq.(12), Eq.(14) and Eq.(19) gives opportunities to group the contribution of all the image sources as will be discussed in next sections.

### A. Reflections between parallel buildings of equal façade heights

The analysis in this section is based on two assumptions. Firstly, it is assumed that the façades are flat, parallel and of equal height. Secondly, only image sources towards the left are considered. As illustrated in Fig. 11, image sources and image receivers extend to

both the left and right side from the real source or real receiver. However, the image sources going further to the "right" need to be diffracted 3 times to reach the receiver and consequently such contributions are much smaller than those going to the left. According to our calculations, the image sources going to the "left" contribute much more than the equivalent image sources going to the "right". When the height of the façades is the same, the contribution of the image sources going to the "right", and similarly, the image receivers going to the "left", can be ignored.

The total contribution is expressed in Eq. (25) if the "left" image source and the "right" image receivers are marked by $l$ and $j$:

$$\sum_{a=0}^{\infty}\sum_{b=0}^{\infty}|p_{a,b}|^2 = |p_{0,0}|^2 + \sum_{a=1}^{\infty}|p_{a,0}|^2 + \sum_{b=1}^{\infty}|p_{0,b}|^2 + \sum_{a=1}^{\infty}\sum_{b=1}^{\infty}|p_{a,b}|^2\,, \tag{25}$$

where the subscripts indicate the positions of the source, the receiver and the image sources and image receivers; $a = 0$ indicates the original source position and $b = 0$ indicates the original receiver position; $a > 0$ and $b > 0$ indicate image sources and image receivers, respectively. $|p_{0,0}|^2$ is the contribution from the pure diffraction path, so involving no reflections. $|p_{a,0}|^2$ is the contribution from the $a^{th}$ image source to the receiver. $|p_{0,b}|^2$ is the contribution from the source to the $b^{th}$ image receiver. $|p_{a,b}|^2$ is the contribution from the $a^{th}$ image source to the $b^{th}$ image receiver.

With these aforementioned assumptions, the level referenced to free field sound

propagation from image source $a$ to the receiver position via the shortest path $L_a$ can be expressed as:

$$\left|\frac{p_{a,0}}{p_{at,L_a}}\right|^2 = \left(\frac{0.37}{X_{a,1}+0.37}\right)^2 \left(\frac{0.37}{X_{a,2}+0.37}\right)^2, \tag{26}$$

where $X_{a,1}$ and $X_{a,2}$ indicate the input from a source and a receiver. When $a > 0$, the sources become virtual, therefore, "1" and "2" are used to indicate "S" and "R" in Eq. (14). For most environmental sounds, the coherence length of the sound is rather short. Moreover, fast temporal changes in propagation conditions may further destroy coherence. Therefore, the phase effect is neglected in Eq. (26) and only the sound power is considered.

For a point source, the sound pressure at distance $L_a$ is $p_{at,L_a} = \frac{S_0}{L_a} e^{-jkL_a}$. $|p_{a,0}|^2$ is rewritten as:

$$|p_{a,0}|^2 = \left(\frac{0.37}{X_{a,1}+0.37}\right)^2 \left(\frac{0.37}{X_{a,2}+0.37}\right)^2 \left(\frac{\rho_s S_0}{L_a}\right)^2, \tag{27}$$

where $\rho_s$ is the reflection coefficient of the façade. For the first image source, the amplitude decreases to $\rho_s S_0$ and for the $a^{th}$ image source, the amplitude decreases to $\rho_s^a S_0$. For diffraction over buildings, the diffraction edge is often around $1.5\pi$. In these cases, $M_\nu(\beta_s - \theta_s) = \frac{\cos\nu\pi - \cos(\beta_s - \theta_s)}{\nu \sin\nu\pi} \approx \frac{\sqrt{3}}{2}\cos\theta_s$ by using the approximation $\cos\frac{2\theta_s}{3} - 0.5 \approx 0.5\cos\theta_s$. The total sum can be written as:

$$|p_{a,0}|^2 = (\rho_s S_0)^2 \left[\frac{0.37}{\sqrt{\frac{2r_{s,a}W}{\lambda(W+r_{s,a})}}\frac{\sqrt{3}}{2}\cos(\theta_{s,a})L_a + 0.37L_a}\right]^2 \left(\frac{0.37}{X_{a,2}+0.37}\right)^2. \quad (28)$$

When $W + r_{s,a} \gg r_r$, $\left(\frac{0.37}{X_{a,2}+0.37}\right)^2 = \left(\frac{0.37}{\sqrt{\frac{2r_r(W+r_{s,a})}{\lambda(r_{s,a}+W+r_r)}}\sqrt{3}(\cos\frac{2}{3}\theta_r - 0.5) + 0.37}\right)^2$ can be approximated as $\left(\frac{0.37}{\sqrt{\frac{2r_r}{\lambda}}\sqrt{3}(\cos\frac{2}{3}\theta_r - 0.5)+0.37}\right)^2$ and becomes independent of the order of the image source and will be called $C_{1s}$. Suppose $r_{s,a} >> W$, Eq. (28) then becomes:

$$|p_{a,0}|^2 \approx (\rho_s S_0)^2 C_{1s} \left(\frac{1}{3.31\sqrt{\frac{W}{\lambda}}h_1 + r_{s,a} + W + r_r}\right)^2, \quad (29)$$

with $h_1$ is the distance from the source to the top of the building. When $r_{s,a}$ is far greater than $H_m$, $L_a \approx d_a + W_s + W + r_r = a\, W_s + 0.5W_s + W + r_r$. The sum over all image sources can be rewritten in a closed form using the Hurwitz-Lerch transcendent:

$$\sum_{a=1}^{\infty} |p_{a,0}|^2 = C_{1s}\,(S_0)^2\,\frac{\rho_s^2}{W_s^2}\Phi\left(\alpha^2 2, \frac{C_{3s}+W_s}{W_s}\right), \quad (30)$$

where $C_{3s} = 0.5W_s + W + r_r + 3.31\sqrt{\frac{W_i}{\lambda}h_1}$; $W_s$ is the width of the source canyon. The details can be found in[15].

Similarly

$$\sum_{b=1}^{\infty} |p_{0,b}|^2 = C_{1r}\,(S_0)^2\,\frac{\alpha^2}{W_r^2}\Phi\left(\rho_r^2 2, \frac{C_{3r}+W_r}{W_r}\right) \quad (31)$$

where $C_{1r} = \left( \frac{0.37}{\sqrt{\frac{2r_s}{\lambda}}\sqrt{3}(\cos\frac{2}{3}\theta_s - 0.5)} \right)^2$ and $C_{3r} = 0.5W_r + W + r_s + 3.31\sqrt{\frac{W}{\lambda}h_2}$. $h_2$ is the distance from the receiver to the top of the building, $\rho_r$ is the reflection coefficient of the receiver canyon. $W_r$ is the width of the receiver canyon.

The $\sum_{b=1}^{\infty}\sum_{a=1}^{\infty}|p_{a,b}|^2$ part is difficult to write in a condensed form, an approximation is given as:

$$\sum_{b=1}^{\infty}\sum_{a=1}^{\infty}|p_{a,b}|^2 \approx \frac{(1.59)^2(\rho_s\rho_r)^6}{\left(\frac{3.31h_1}{\sqrt{\lambda}+1.5W_s+W+1.5W_r}\right)\left(\frac{3.31h_3}{\sqrt{\lambda}+1.5W_s+W+1.5W_r}\right)}. \quad (32)$$

The details could be found in[15].

To validate the aforementioned approaches and simplifications, a comparison is made with full-wave FDTD calculations[25;26], taking $W_s = 20$, $h_1 = 11$, $W = 10$, $h_3 = 11$, $\beta_s = \beta_r = 1.5\pi$, $\phi_s = 0.25\pi$, $H_r = 0$ (see Fig. 13). Ground reflections are not considered and the source is positioned in the middle of the source canyon. The configuration studied is summarized in Fig. 14 (a).

More specifically, Fig. 13 shows the differences between the FDTD simulations and the results calculated using Eq. (25). Since the FDTD simulations are in 2D, in order to limit the computational burden, the simulated time signal is multiplied by $\frac{1}{\sqrt{ct}}$ to transfer the response of a (coherent) line source to the one of a point source as proposed in[27]. The results of four individual frequencies are depicted. The overestimation near the extension

line of the roof top originates from the diffraction model as presented in the previous sections. The errors at the other receiver positions can be considered as the uncertainties caused by the reflection model combined with diffraction.

## B. Generalize the reflections combined with multiple diffraction

The combination of reflections and multiple diffractions will be discussed in this section. The facade heights $h_1$ and $h_3$, see Fig. 14, play an important role now.

***Façades with equal height:*** $h_1 = h_3$

According to Eq.(18), the squared sound pressure after $n-1$ diffractions over the squared sound pressure in free field can be written as:

$$\left|\frac{p_{n-1}^{S1\cdots n}}{p_{at,L}}\right|^2 = \left(\frac{1}{2}\right)^{2C} \prod_{l=1}^{n-1} |D_l|^2 \quad n = 2, 3, \cdots . \tag{33}$$

Substituting Eq.(19) and Eq.(24) into Eq. (33) and moving the first diffraction term out of the product leads to:

$$\left|\frac{p_{a,0}}{p_{at,L_a}}\right|^2 = \left(\frac{1}{2}\right)^{2C}\left(\frac{0.37}{0.37+\sqrt{\frac{2W_{12}r_{s,a}}{\lambda(W_{12}+r_{s,a})}}M_{\nu 1}(\theta_{1+})}+\frac{0.37}{0.37+\sqrt{\frac{2W_{12}r_{s,a}}{\lambda(W_{12}+r_{s,a})}}M_{\nu 1}(\theta_{1-})}\right)^2 \prod_{l=2}^{n-1}\left(\frac{0.37}{0.37+\sqrt{\frac{2W_{l,l+1}(r_{s,a}+\sum_{j=1}^{l-1}W_{j,j+1})}{\lambda(r_{s,a}+\sum_{j=1}^{l}W_{j,j+1})}}M_{\nu l}(\theta_{l+})}+\frac{0.37}{0.37+\sqrt{\frac{2W_{l,l+1}(r_s+\sum_{j=1}^{l-1}W_{j,j+1})}{\lambda(r_s+\sum_{j=1}^{l}W_{j,j+1})}}M_{\nu l}(\theta_{l-})}\right)^2. \quad (34)$$

If the first two diffraction edges are adjacent to each other, which means that sounds do not propagate over a thin barrier first, $M_{\nu 1}(\theta_{1+}) = M_{\nu 1}(\theta_{1-})$. For a rectangular building, the diffraction angle $\beta_{s,1}$ is $1.5\pi$, $M_\nu(\beta_{s,1}-\theta_{s,1}) = \frac{\cos\nu\pi-\cos(\beta_{s,1}-\theta_{s,1})}{\nu\sin\nu\pi} \approx \frac{\sqrt{3}}{2}\cos\theta_{s,1}$. Also, if $r_s+\sum_{j=1}^{l-1}W_{j,j+1}$ is much greater than $W_{l,l+1}$, $\frac{r_{s,a}+\sum_{j=1}^{l}W_{j,j+1}-W_{l,l+1}}{(r_{s,a}+\sum_{j=1}^{l}W_{j,j+1})}$ approaches 1. Eq.(34) can further be reduced to:

$$\left|\frac{p_{a,0}}{p_{at,L_a}}\right|^2 \approx \left(\frac{1}{2}\right)^{2C-2}\left(\frac{0.37}{0.37+\sqrt{\frac{2W_{12}r_{s,a}}{\lambda(W_{12}+r_{s,a})}}\frac{\sqrt{3}}{2}\cos\theta_{s,1}}\right)^2 \prod_{l=2}^{n-1}\left(\frac{0.37}{0.37+\sqrt{\frac{2W_{l,l+1}}{\lambda}}M_{\nu l}(\theta_{l+})}+\frac{0.37}{0.37+\sqrt{\frac{2W_{l,l+1}}{\lambda}}M_{\nu l}(\theta_{l-})}\right)^2. \quad (35)$$

Multiplying both sides of the above equation with $|p_{at,L_a}| = \frac{S_0\rho_s^a}{L_a}$, the total contribution can be written in a generalized form. On condition that the angle of the

diffracting edge is $1.5\pi$ (rectangular building), the approximation used in Eq.(28) is still satisfied, and the above equation becomes:

$$\begin{aligned}\sum_{a=1}^{\infty}|p_{a,0}|^2 &= C_{1,g}\sum_{a=1}^{\infty}\left[(S_0\rho_s^a)^2\Big(\frac{0.37}{L_a+\sqrt{\frac{2W_{12}r_{s,a}}{\lambda(W_{12}+r_{s,a})}}\frac{\sqrt{3}}{2}\cos\theta_{s,1}L_a}\Big)^2\right]\\ &= C_{1,g}\sum_{a=1}^{\infty}\left[(S_0\rho_s^a)^2\Big(\frac{1}{L_a+3.31h_1\sqrt{\frac{W_{12}}{\lambda}\frac{(r_{s,a}+\sum_{j=1}^{l-1}W_{j,j+1}+r_r)^2}{r_{s,a}(W_{12}+r_{s,a})}}}\Big)^2\right], \quad (36)\end{aligned}$$

where

$$C_{1,g}=\left(\frac{1}{2}\right)^{2C-2}\prod_{l=2}^{n-1}\left(\frac{0.37}{0.37+\sqrt{\frac{2W_{l,l+1}}{\lambda}}M_{\nu l}(\theta_{l+})}+\frac{0.37}{0.37+\sqrt{\frac{2W_{l,l+1}}{\lambda}}M_{\nu l}(\theta_{l-})}\right)^2. \quad (37)$$

Suppose $r_{s,a}$ is much greater than $\sum_{j=1}^{l-1}W_{j,j+1}+r_r$, $\sqrt{\frac{(r_{s,a}+\sum_{j=1}^{l-1}W_{j,j+1}+r_r)^2}{r_{s,a}(W_{12}+r_{s,a})}}$ can be approximated as 1. The uncertainties of this assumption will be discussed later. With this assumption, Eq. (36) can be similarly calculated as before with the Hurwitz-Lerch transcendent:

$$\sum_{a=1}^{\infty}|p_{a,0}|^2=C_{1,g}\,(S_0)^2\,\frac{\alpha^2}{W_s^2}\Phi(\alpha^2,2,\frac{C_{3,g}+W_s}{W_s}), \quad (38)$$

where

$$C_{3,g} = 3.31\sqrt{\frac{W_{12}}{\lambda}}h_1 + 0.5W_s + r_r + \sum_{j=1}^{n-1} W_{j,j+1}. \tag{39}$$

When $n = 2$, $C_{1,g} = C_{1,s}$ and $C_{3,g} = C_{3,s}$.

The test case in Fig. 14 (b) is used to validate the generalized form for $h_1 = h_3$. The predicted errors (see Fig. 15) are relative large compared to the previous validation cases. The possible reasons will be discussed in section IV.

***Façades with different heights:*** $h_3 < h_1$

If $h_3 < h_1$, some of the image sources located away from the screening building cannot contribute anymore to the total sound pressure level without an additional diffraction as shown by the dashed line in Fig. 16 (a). Accordingly, the image sources located in the direction of the central building become more relevant. Assuming that the source lies in the middle of the canyon $W_s$ and according to the simple ratio $\frac{aW_s+0.5W_s}{h_1} = \frac{aW_s-0.5W_s}{h} = 1, 2, \cdots$, the relation between $h$ and $h_1$ is $h = \frac{a-0.5}{a+0.5}h_1$, where $h_1 = H_m-$source height. When $h = \frac{a-0.5}{a+0.5}h_1 > H_s-$ source height, the $a$th image source will become unavailable. Specifically, the relation actually is $h = 1/3h_1$, $1/3h_1$, $3/5h_1$, $5/7h_1 \cdots$.

Instead of $\sum_{a=1}^{\infty} |p_{a,0}|^2$, the total contribution becomes:

$$\begin{aligned}
&\sum_{a=1}^{N}|p_{a,0}|^2+\sum_{a=N+1}^{\infty}|q_{a,0}|^2=\sum_{a=1}^{\infty}|p_{a,0}|^2-\sum_{a=N+1}^{\infty}|p_{a,0}|^2+\sum_{a=1}^{\infty}|q_{a,0}|^2\\
=\;& C_{1,g,1}S_0^2\frac{\alpha^2}{W_s^2}\Phi(\alpha^2,2,1+\frac{C_{3,g,1}}{W_s})-C_{1,g,1}S_0^2\frac{\alpha^2}{W_s^2}\Phi(\alpha^2,2,N+1+\frac{C_{3,g,1}}{W_s})\\
+\;& C_{1,g,2}S_0^2\frac{\alpha^2}{W_s^2}\Phi(\alpha^2,2,1+\frac{C_{3,g,2}}{W_s}),
\end{aligned}\tag{40}$$

where $|p_{a,0}|^2$ and $|q_{a,0}|^2$ are used to distinguish different diffracted sound paths. $N$ is the number indicating image sources that need to be diffracted 3 times to reach the receiver. $p_{a,0}$ is sound diffracted twice and $q_{a,0}$ is sound diffracted 3 times to reach the receiver position. $C_{1,g,x}$ and $C_{3,g,x}$ can be calculated by Eq.(37) and Eq.(39). The indices "$x$" of $C_{1,g}$ and $C_{3,g}$ are used to distinguish between different inputs in Eq.(37) and Eq.(39).

The configuration depicted in Fig. 16 (a) is used to validate Eq.(40). The errors at most receivers are less than 2 dB as shown in Fig. 17. The largest deviations from the full-wave reference calculations appear near the extension line of the building's roof.

***Façades with different heights:*** $h_3 > h_1$

If $h_3 > h_1$, the contribution of the diffraction for paths such as "$S \to 2 \to 1 \to 3 \to R$", "$S \to 1 \to 3 \to R$" and "$S \to 1 \to R$" (see Fig. 16 (b)) may not be neglected. The recommended formula for a configuration where $h_3 > h_1$ is:

$$
\begin{aligned}
& \sum_{a=1}^{\infty} |p_{a,0}|^2 + \sum_{a=1}^{M} |q_{a,0}|^2 + \sum_{a=M+1}^{N} |q_{a,0}|^2 + \sum_{a=N+1}^{\infty} |q_{a,0}|^2 \\
= \; & C_{1,g,3} S_0^2 \frac{\alpha^2}{W_s^2} \Phi(\alpha^2, 2, 1 + \frac{C_{3,g,3}}{W_s}) + \sum_{a=1}^{M} |q_{a,0}|^2 + \sum_{a=M+1}^{N} |q_{a,0}|^2 \\
+ \; & C_{1,g,4} S_0^2 \frac{\alpha^2}{W_s^2} \Phi(\alpha^2, 2, 1 + \frac{C_{3,g,4}}{W_s}) - C_{1,g,4} S_0^2 \frac{\alpha^2}{W_s^2} \Phi(\alpha^2, 2, N + 1 + \frac{C_{3,g,4}}{W_s}), \qquad (41)
\end{aligned}
$$

where $C_{1,g,3}$, $C_{3,g,3}$, $C_{1,g,4}$ and $C_{3,g,4}$ can be calculated from the generalized form of Eq.(37) and Eq.(39). $M$ is the image source number from which the diffraction path changes from $S \to 1 \to R$ to $S \to 1 \to 3 \to R$. $N$ is the image source number from which the diffraction path changes from $S \to 1 \to 3 \to R$ to $S \to 1 \to 2 \to 3 \to R$. Since $M$ and $N$ are often small numbers, the contributions of these cases can be explicitly summed.

The results of the test case are shown in Fig. 18. Levels at most receivers agree well with the simulations. In contrast to conditions $h_1 = h_3$ and $h_3 < h_1$, the predicted levels are now smaller than with the full-wave simulations.

## IV. Discussion

By introducing several approximations, urban sound propagation involving multiple reflections and diffractions is highly simplified and the calculation speed is improved by several orders of magnitude. The most important steps are the introduction of an approximation for the Fresnel Integral, the assumption that the effect of multiple

diffraction can be approximated by including only the shortest path connection all rooftops, and by compacting the sum over all image sources caused by the source and receiver canyon reflections. The first approximation has been validated by comparison with a full analytical model, the others by comparison to full-wave FDTD simulations.

The error introduced by the approximation of the Fresnel Integral remains smaller than one dB except near the edge of the shadow region. The error introduced by approximating the Fresnel Integral in case of multiple diffraction behaves very similar. It should nevertheless be noted that this does not check the validity of taking into account the shortest path only.

Approximating the sum over multiple image sources allows obtaining a closed analytical form for the sum. Two approximations used to resolve the sum were presented. The first one allows eliminating the image source location from all diffraction terms except from the first one. This requires that $r_s + \sum_{j=1}^{l-1} W_{j,j+1}$ is much greater than $W_{l,l+1}$. The second assumption states that $r_{s,a} \gg \sum_{j}^{n-1} W_{j,j+1} + r_r$, which means that $\frac{r_{s,a}+\sum_{j=1}^{n-1} W_{j,j+1}+r_r}{r_{s,a}} \approx 1$. However, this condition maybe not satisfied for long-distance propagation in combination with a source located in a narrow canyon. If $\sum_{j}^{n-1} W_{j,j+1} + r_r < 500\text{m}$, the error caused by $\frac{r_{s,a}+\sum_{j=1}^{n-1} W_{j,j+1}+r_r}{r_{s,a}} \approx 1$ is less than 3 dB in an urban setting.

Moreover, if this distance is larger than 500 m, one will often encounter other noise

sources at closer distance, dominating the overall noise climate. For shorter distances, the impact of the approximation was explicitly tested by comparing levels calculated with the simplified analytical model to numerical simulations. This showed that in the deep shadow region errors are generally lower than 1 dB even in the case of multiple intermediate buildings.

In real urban situations, some particular cases may occur that are not explicitly covered by the formulations presented in this paper. For example, in Fig. 19 (a), the depicted image source reaches the receiver by interacting with different building edges than e.g. the (original) source. Another typical case is shown in Fig. 19 (b): the left building is higher than the right one and the receiver is far away. Some of the image sources could reach the receiver by a single diffraction only. Therefore, carefully analysing the contributions from the different image sources is needed when using such theoretical diffraction formulas.

While deriving the model, an important assumption is that the source is located in the middle of the source canyon, which is representative for typical road traffic noise sources. These assumptions allowed simplifying the presented diffraction model. Deviations from these will lead to less accurate results. Ground reflections are not considered either. However, these can be easily incorporated by using an additional set of image sources located below the ground plane. Similar formulas as represented here can be used.

Compared to explicitly summing up the image source contributions, the Hurwitz-Lerch transcendent is more efficient if the number of image sources is greater than 3. Fig. 20 (a) shows the ratio of calculating time between these two approaches. This comparison is based on reflections in a souce canyon followed by diffraction over a rectangular building of 10 m wide. Each data point on the y-axis is the average of running the engineering models for 100 times. From this figure it can bee seen that the calculating times are similar for the model presented in this work, the ISO9613-2 model, the CNOSSOS-EU model, and the HARMONOISE model. Only the NORD2000 model is significantly slower.

In addition, Fig. 20 (b) shows the accuracy of diffracted sound over an isolated thick barrier using these models. The source is at 4.8 m from the barrier façade and at 10 m from its top. The receiver is at 4.5 m from the barrier façade and at 6.6 m from the barrier top. The model presented in this work, Pierce's model, and NORD2000 yield accurate predictions when comparing with the FDTD simulations. The ISO9613-2, the CNOSSOS-EU and the HARMONOISE model overestimate the sound pressure levels.

## V. Conclusion

A simplified method to predict sound pressure levels at shielded areas in typical urban situations are presented and validated. This method is essentially based on Pierce's diffraction theory, where the Fresnel Integral is approximated by a special pair of trigonometric functions tuning this approximation to typical situations encountered in

urban sound propagation: tall barriers and a specific interest in the deep shadow zone. The new single, double and multiple diffraction functions are validated by theoretical solutions and full-wave simulations. Although the error that is introduced is limited to below 1 dB in most of the zones of interest, the gain in calculation time is huge (several orders of magnitude). This paper focused in particular on combining the effect of multiple reflections with multiple diffraction. Additional assumptions allow making a significant part of the sum independent of the reflection order and independent of the infinite sum of image sources; the contribution of the image sources can be relatively easily condensed with the Hurwitz-Lerch transcendent. Once this sum contains more than 3 image sources, some additional calculation time is gained by this last step. Generally, the new method can predict sound pressure levels at shielded urban areas, within 2 dB compared with numerical simulations in most of the receiver positions, with a low computing cost.

## REFERENCES

**1.** J. B. Keller, "Geometrical Theory of Diffraction," J. Acoust. Soc. Am. 52, 116-130 (1962).

**2.** R.G. Kouyoumjian and P.H. Pathak, "A uniform geometrical theory of diffraction for an edge in a perfectly conducting surface," *Proceedings of the IEEE*, 62, 1448-1461 (1974).

**3.** A. D. Pierce, "Diffraction of sound around corners and over wide barriers," J. Acoust. Soc. Am. 55, 941-955 (1974).

**4.** A. D. Pierce, *Acoustics: An Introduction to Its Pysical Principles and Applications.* Acoustical Society of America, New York, USA, 1989.

**5.** T. Kawai, "Sound diffraction by a many-sided barrier or pillar," J. Sound Vib. 79, 229-242 (1981).

**6.** H.-S. Kim, J.-S. Kim, H.-J. Kang, B.-K. Kim, and S.-R. Kim, "Sound diffraction by multiple wedges and thin screens," Appl. Acoust. 66, 1102-1119 (2005).

**7.** H. Min and X. Qiu, "Multiple acoustic diffraction around rigid parallel wide barriers," J. Acoust. Soc. Am. 126, 179-186 (2009).

**8.** Y. W. Lam and S. C. Roberts, "A simple method for accurate prediction of finite barrier insertion loss," J. Acoust. Soc. Am. 93, 1445-1452 (1993).

**9.** I. Tolstoy, Diffraction by a hard truncated wedge and a strip," IEEE J. Oceanic Eng. 14, 4-16 (1989).

**10.** I. Tolstoy, "Exact, explicit solutions for diffraction by hard sound barriers and seamounts," J. Acoust. Soc. Am. 85, 661-669 (1989).

**11.** D. Ouis, "Noise attenuation by a hard wedge-shaped barrier," J. Sound Vib. 262, 347-364 (2003).

**12.** K.M. Li and H.Y. Wong, "A review of commonly used analytical and empirical formulae for predicting sound diffracted by a thin screen," Appl. Acoust. 66, 45-76 (2005).

**13.** G. J. Wadsworth and J. P. Chambers, "Scale model experiments on the insertion loss of wide and double barriers," J. Acoust. Soc. Am. 107, 2344-2350 (2000).

**14.** Y. Berthelot and J. Zhou, "Scale-Model Experiments on the Validity of the Matched Asymptotic Expansions Theory for Sound Diffraction by Curved Surfaces of Finite Impedance," J. Acoust. Soc. Am. 93, 605-608 (1993).

**15.** W. Wei, D. Botteldooren, T. Van Renterghem, M. Hornikx, J. Forssén, E. Salomons, and M. Ögren, "Urban background noise mapping: The general model," Acta Acust. united Ac. 100, 1098-1111 (2014).

**16.** K. Heutschi, "A simple method to evaluate the increase of traffic noise emission level due to buildings, for a long straight street," Appl. Acoust. 44, 259-274 (1995).

**17.** P. Thomas, T. Van Renterghem, E. De Boeck, L. Dragonetti, and D. Botteldooren,

"Reverberation-based urban street sound level prediction," J. Acoust. Soc. Am. 133, 3929-3939 (2013).

**18.** D. Chu and T. K. Stanton, "Higher order acoustic diffraction by edges of finite thickness," J. Acoust. Soc. Am. 116, 2566-2566 (2004).

**19.** K. D Mielenz, "Computation of fresnel integrals. II," J. Res. Natl. Inst. Stand. Technol. 105 (2000).

**20.** J. Defrance, E. Salomons, I. Noordhoek, D. Heimann, B. Plovsing, G. Watts, H. Jonasson, X. Zhang, E. Premat, I. Schmich, F. Aballea, M. Baulac, and F. de Roo, "Outdoor sound propagation reference model developed in the european harmonoise project," Acta Acust. united Ac. 93, 213-227 (2007).

**21.** E. Salomons, D. van Maercke, J. Defrance, and F. de Roo, "The harmonoise sound propagation model," Acta Acust. united Ac. 97, 62-74 (2011).

**22.** Environmental noise and the CNOSSOS-EU initiative, 2012.

**23.** E. Salomons, H. Polinder, W. Lohman, H. Zhou, H. Borst, and H. Miedema, "Engineering modeling of traffic noise in shielded areas in cities," J. Acoust. Soc. Am. 126, 2340-2349 (2009).

**24.** W. Kropp, J. Forssén, M. Ögren, and P. Thorsson, "The failure of traditional traffic

noise control for quiet areas," *Proceedings of Inter-Noise 2004*, Prague, Czech Republic, 2004.

**25.** D. Botteldooren, "Finite-difference time-domain simulation of low-frequency room acoustic problems," J. Acoust. Soc. Am. 98, 3302-3308 (1995).

**26.** T. Van Renterghem and D. Botteldooren, "Prediction-step staggered-in-time fdtd: An efficient numerical scheme to solve the linearised equations of fluid dynamics in outdoor sound propagation," Appl. Acoust. 68, 201-216 (2007).

**27.** K. Heutschi, "Calculation of reflections in an urban environment," Acta Acust. united Ac. 95, 644-652 (2009).

# Figure Captions

Figure 1. Geometry and dimensions of single-wedge (a), double-edge (b) and multiple (c)-(d) diffraction.

Figure 2. Comparison of the approximation accuracy of Fresnel Integral $C(x)$ and $S(x)$.

Figure 3. Distribution of $X$ from two European cities. The meaning of $X_{i+}$ and $X_{i-}$ is explained in Eq.(2). The values shown in this figure are from vertical cross sections based on a 2.5D approach to noise mapping.

Figure 4. Comparison of a single (a) and double (b) diffraction case, using Pierce's method and the "simplified" set of equations introduced in this paper. Parameters for the single wedge diffraction are $r_s = r_r = 1\lambda, 10\lambda$ and $100\lambda$ (up to down), respectively, $\beta = 11/6\pi$, $\theta_s = \pi/6$, for varying $\theta$. For the double diffraction calculations, $r_s = r_r = W = 1\lambda, 10\lambda$ and $100\lambda$ (up to down), respectively, $\beta_s = \beta_r = 1.5\pi$, $\theta_s = \pi/4$, for varying $\theta_r$.

Figure 5. Comparison of calculation efficiency between Pierce's diffraction solution and the simplified method presented in this work. The results are based on running the algorithms 10000 times. The algorithm used for calculating the Fresnel Integral is based on[19], using 12 terms in the Taylor series expansion.

Figure 6. Geometries considered to validate multiple diffractions in absence of a source and receiver canyon.

Figure 7. Contour plots showing the sound pressure level difference between the presented simplified method and Pierce's solution ($L_{simplified} - L_{Pierce}$) in the receiver zone as defined in Fig. 6, for configuration (a). Calculations were performed for a sound frequency of 250 Hz (left) and 2000 Hz (right). (Color online)

Figure 8. See caption of Fig. 7, but now for the configuration shown in Fig. 6 (b). (Color online)

Figure 9. See caption of Fig. 7, but now for the configuration shown in Fig. 6 (c). (Color online)

Figure 10. See caption of Fig. 7, but now for the configuration shown in Fig. 6 (d). (Color online)

Figure 11. Location of image sources (open circles) and image receivers (open triangles). Reflections from the ground are not considered.

Figure 12. Effect of facade reflections (no ground reflections), for the case shown in Fig. 14 (a). In part (a), $W_s = 22$ m; $h_1 = 10$ m; $r_r = 7$ m; $W_i = 22$ m; $\beta_s = \beta_r = 1.5\pi$; the wave length is equal to 0.68 m (500 Hz); the source is located in the middle of the canyon. Sound pressure levels are shown relative to free field sound propagation. In part (b), the same parameters are used as in (a), but $W_s$ and $h_1$ vary in the typical urban setting range;

the facade reflection coefficient is equal to 0.97. The level difference is the increase between many image sources and a single image source only. (Color online)

Figure 13. Contour plots of level difference between the simplified model (including multiple reflections and double diffraction) and FDTD simulations at 4 sound frequencies, for the case depicted in Fig. 14 (a). (Color online)

Figure 14. Cases considered (a) including reflections in the source canyon followed by double diffraction; (b) is a generalized case including reflections in the source canyon and multiple diffractions.

Figure 15. Contour plots of the level difference between the generalized, simplified model and the FDTD simulations for the geometry as shown in Fig. 14 (b) with $h_1 = h_3 = 11$ m and $W_s = 20$ m, at 4 sound frequencies. (Color online)

Figure 16. Analysis of sound paths in case of $h_3 < h_1$ (a) or $h_3 > h_1$ (b).

Figure 17. Contour plot of the level difference between the generalized, simplified model and the FDTD simulations for the geometry as shown in Fig. 16 (a) with $W_s = 20$ m, $W = 10$ m, $h_1 = 11$ m and $h_3 = 7$ m. (Color online)

Figure 18. Contour plot of the level difference between the generalized, simplified model and the FDTD simulations for the geometry as shown in Fig. 16 (b) with $W_s = 20$ m, $W = 10$ m, $h_1 = 7$ m and $h_3 = 11$ m. (Color online)

Figure 19. Two particular cases not explicitly covered by the formulations presented in this work.

Figure 20. Comparison of computational efficiency and numerical accuracy of the simplified model developed in this work and various engineering type models; (a) CPU time ratio between explicitly summing up image source contributions and application of the Hurwitz-Lerch transcendent; (b) comparison of the sound pressure levels, relative to free field sound propagation, by applying different engineering models and full-wave calculations, at sound frequencies ranging from 31.5 Hz to 1 kHz.

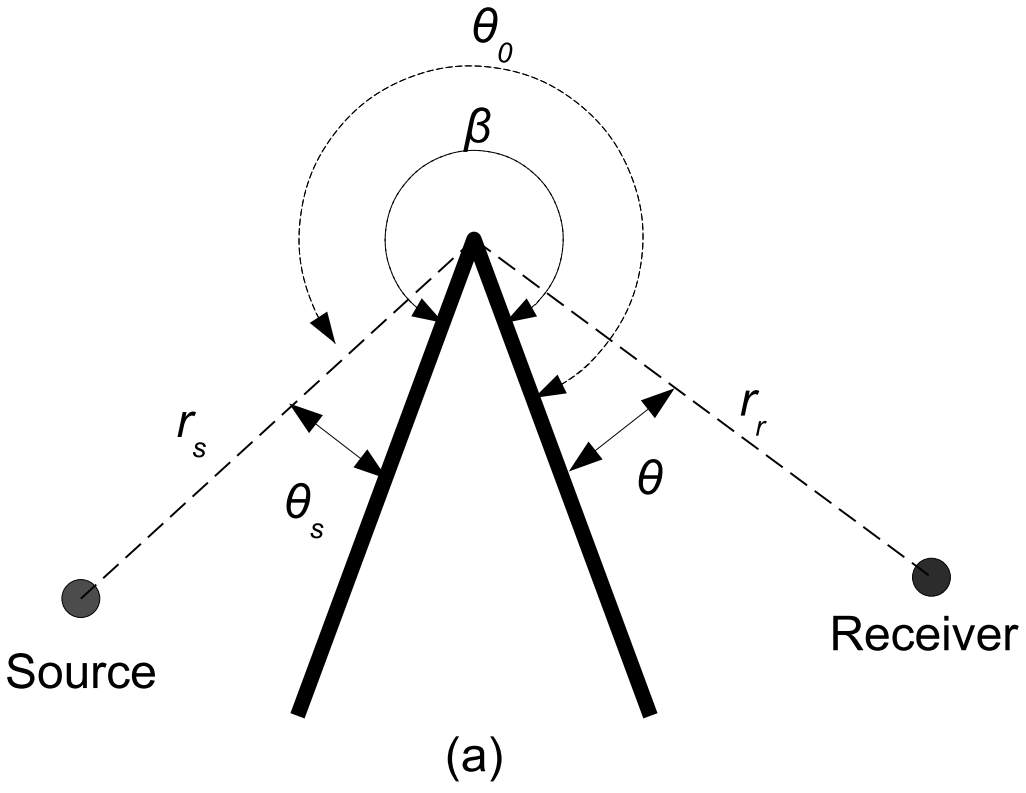
θ0
β
rs
θs
θ
rr
Source
Receiver

(a)

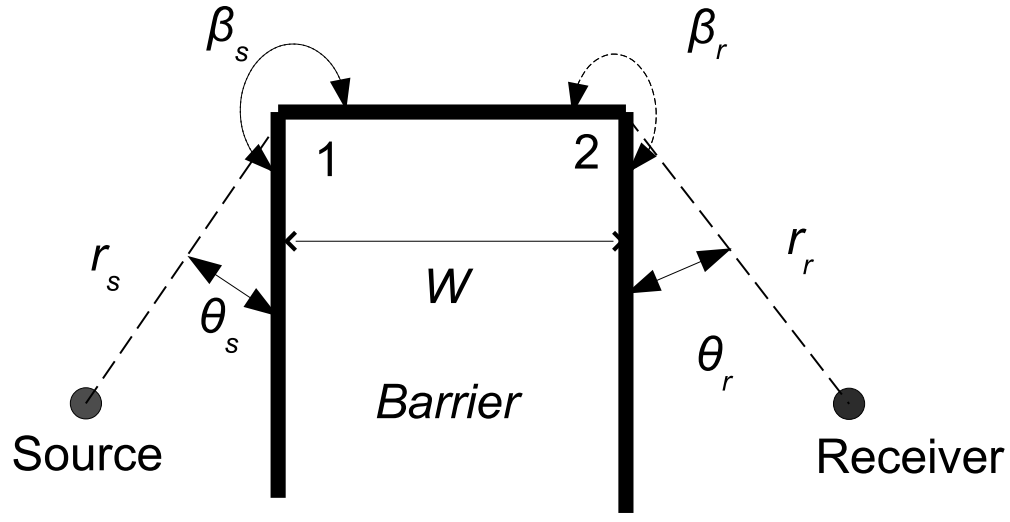
βs
βr
1
2
rs
W
rr
θs
θr
Barrier
Source
Receiver

(b)

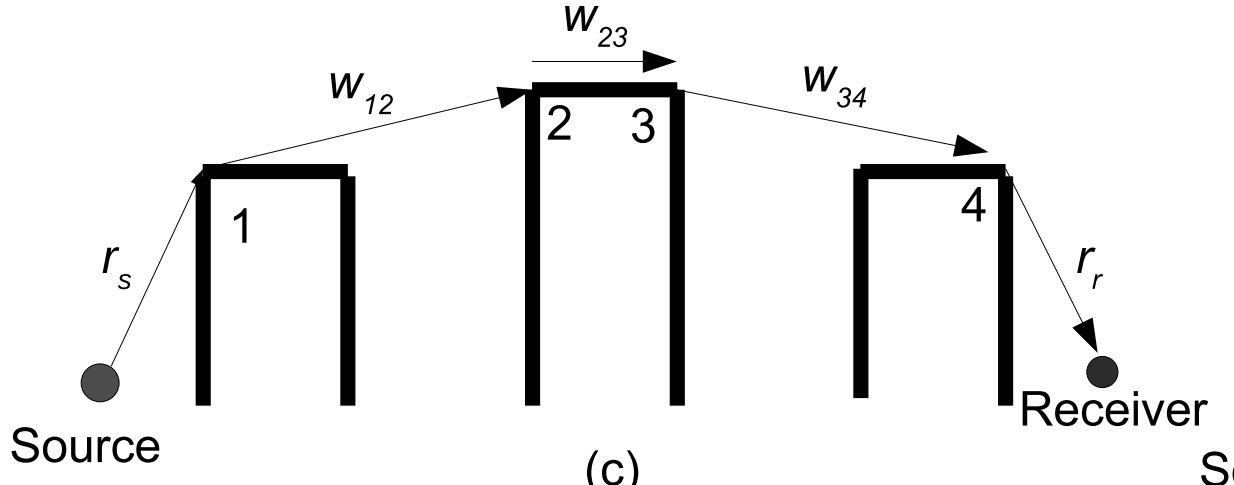
w23
w12
w34
2
3
1
4
rs
rr
Source
Receiver

(c)

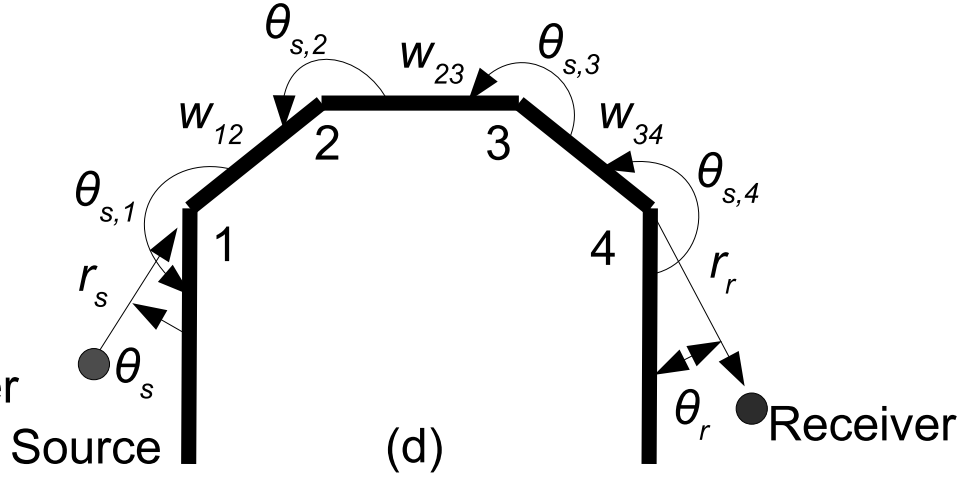
θs,2
w23
θs,3
w12
w34
θs,4
θs,1
2
3
1
4
rr
rs
θs
θr
Source
Receiver

(d)

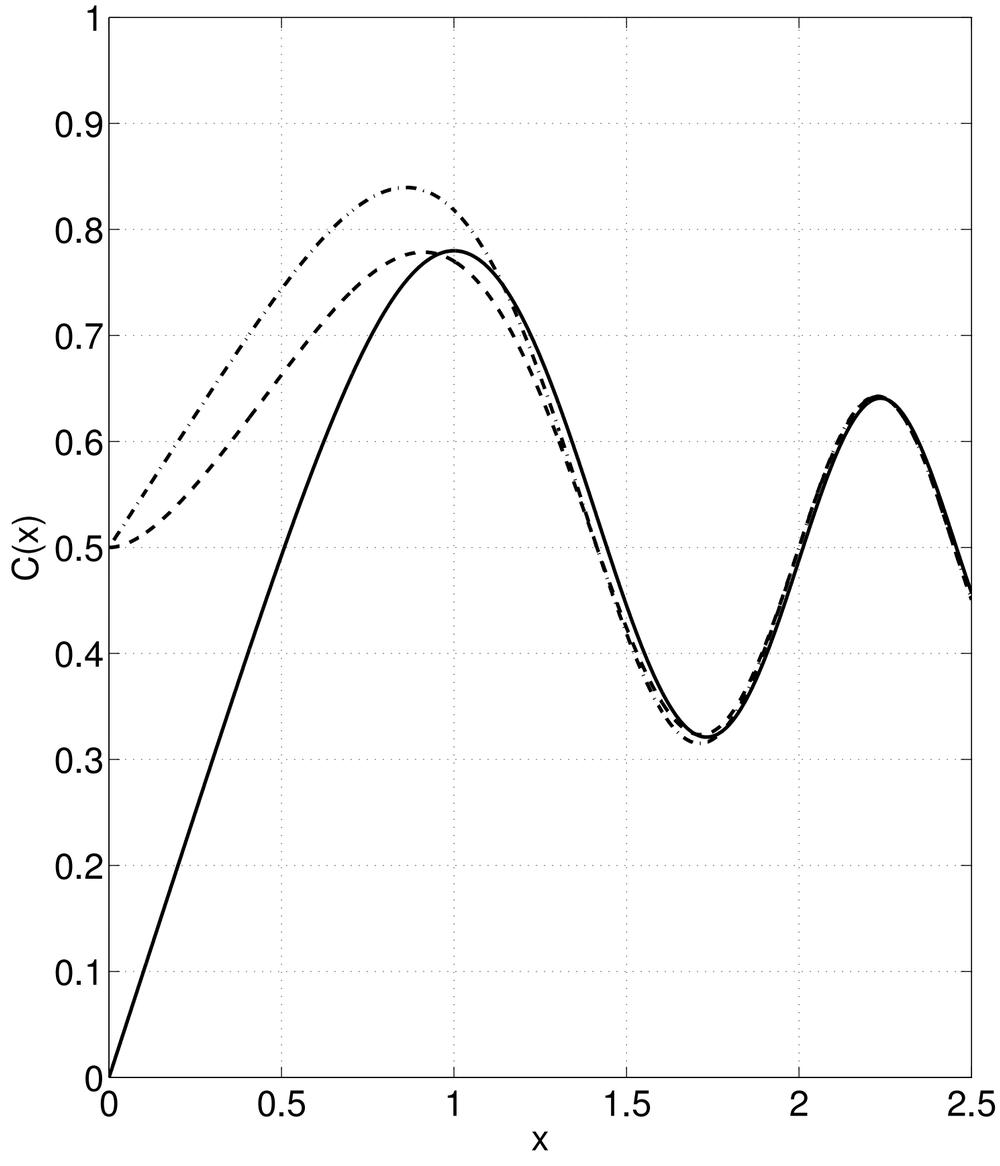
C(x)
x
0
0.1
0.2
0.3
0.4
0.5
0.6
0.7
0.8
0.9
1
0
0.5
1
1.5
2
2.5

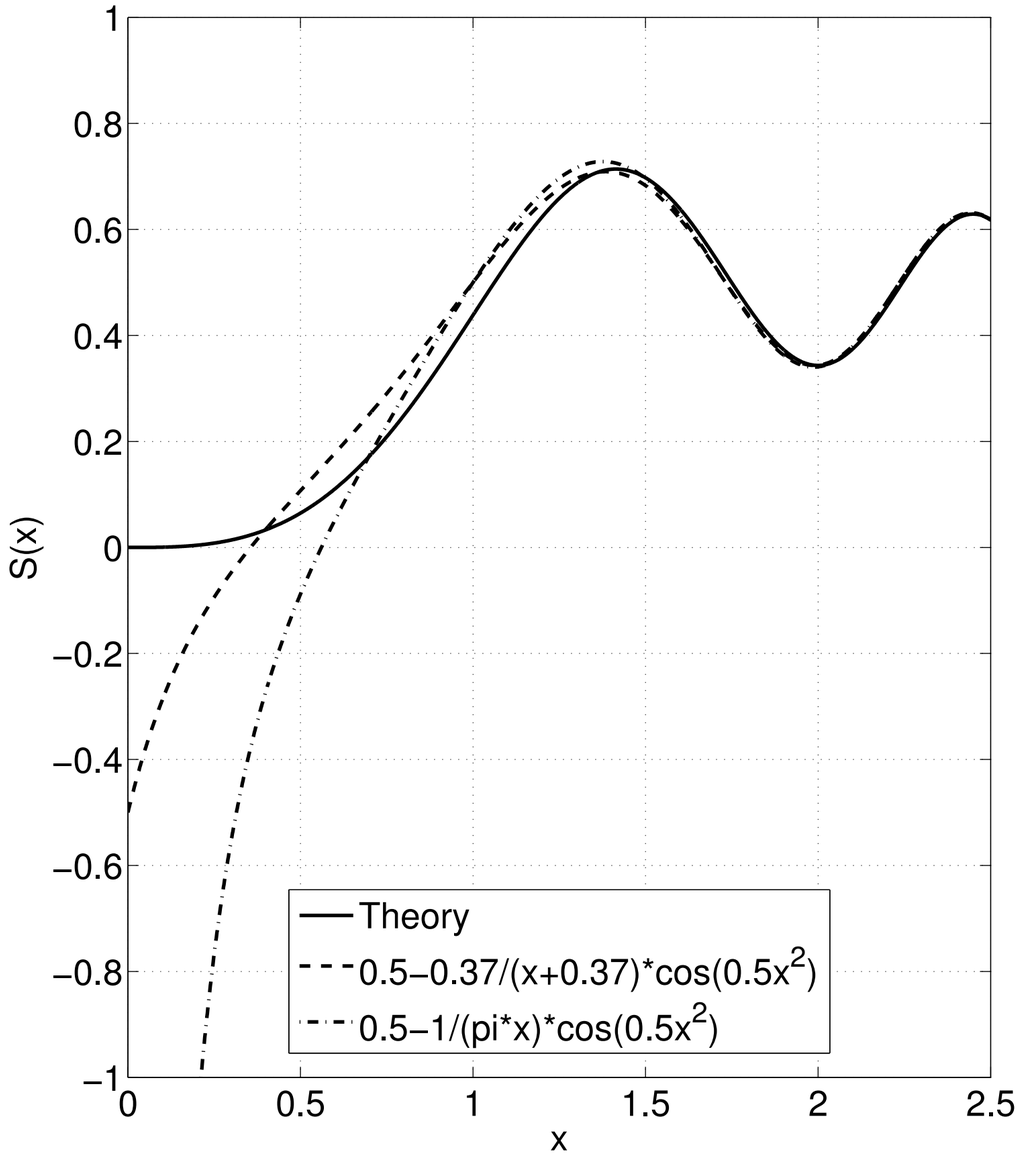
S(x)
x
Theory
0.5−0.37/(x+0.37)*cos(0.5x^2)
0.5−1/(pi*x)*cos(0.5x^2)
−1
−0.8
−0.6
−0.4
−0.2
0
0.2
0.4
0.6
0.8
1
0
0.5
1
1.5
2
2.5

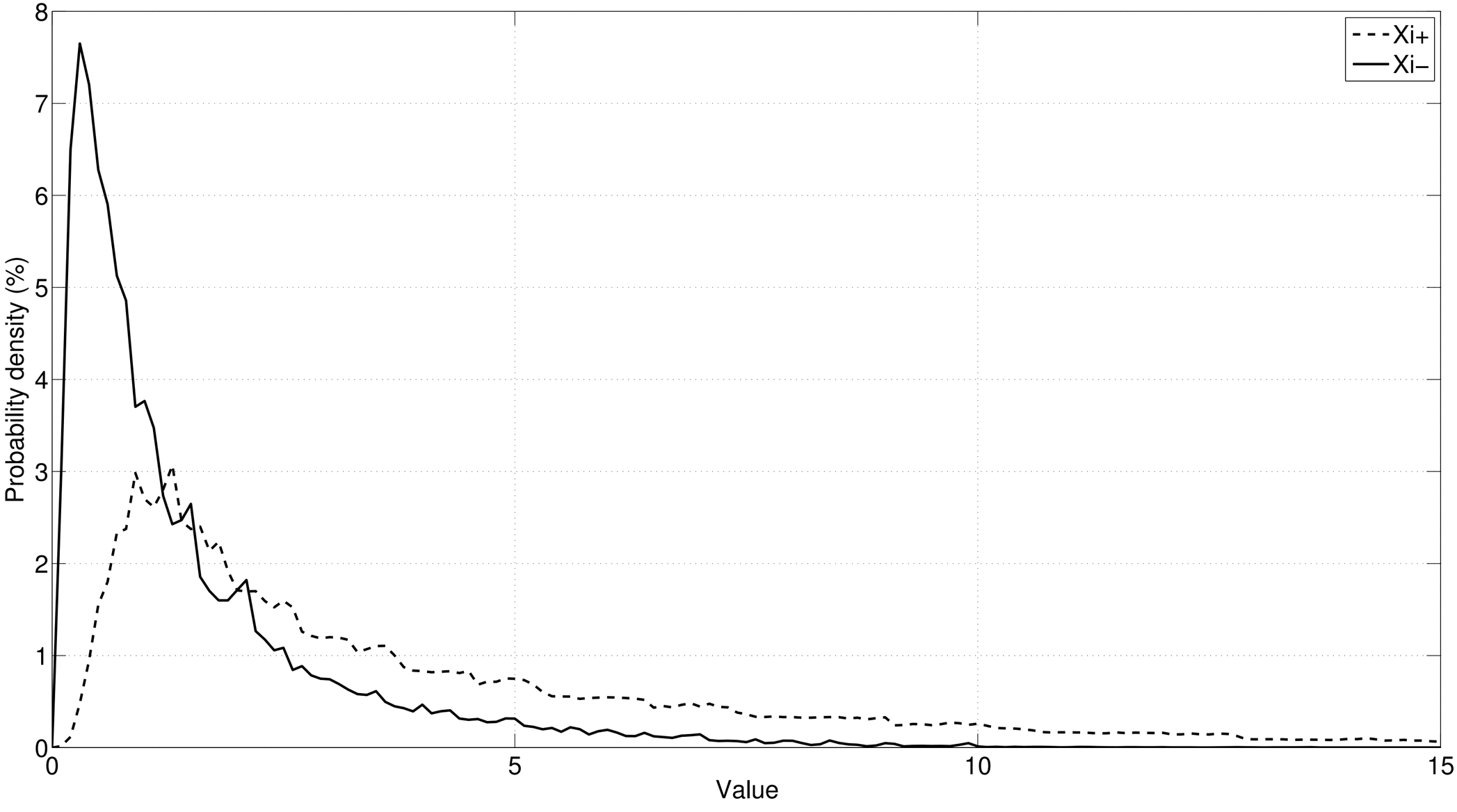
Xi+
Xi−
Probability density (%)
Value
0
1
2
3
4
5
6
7
8
0
5
10
15

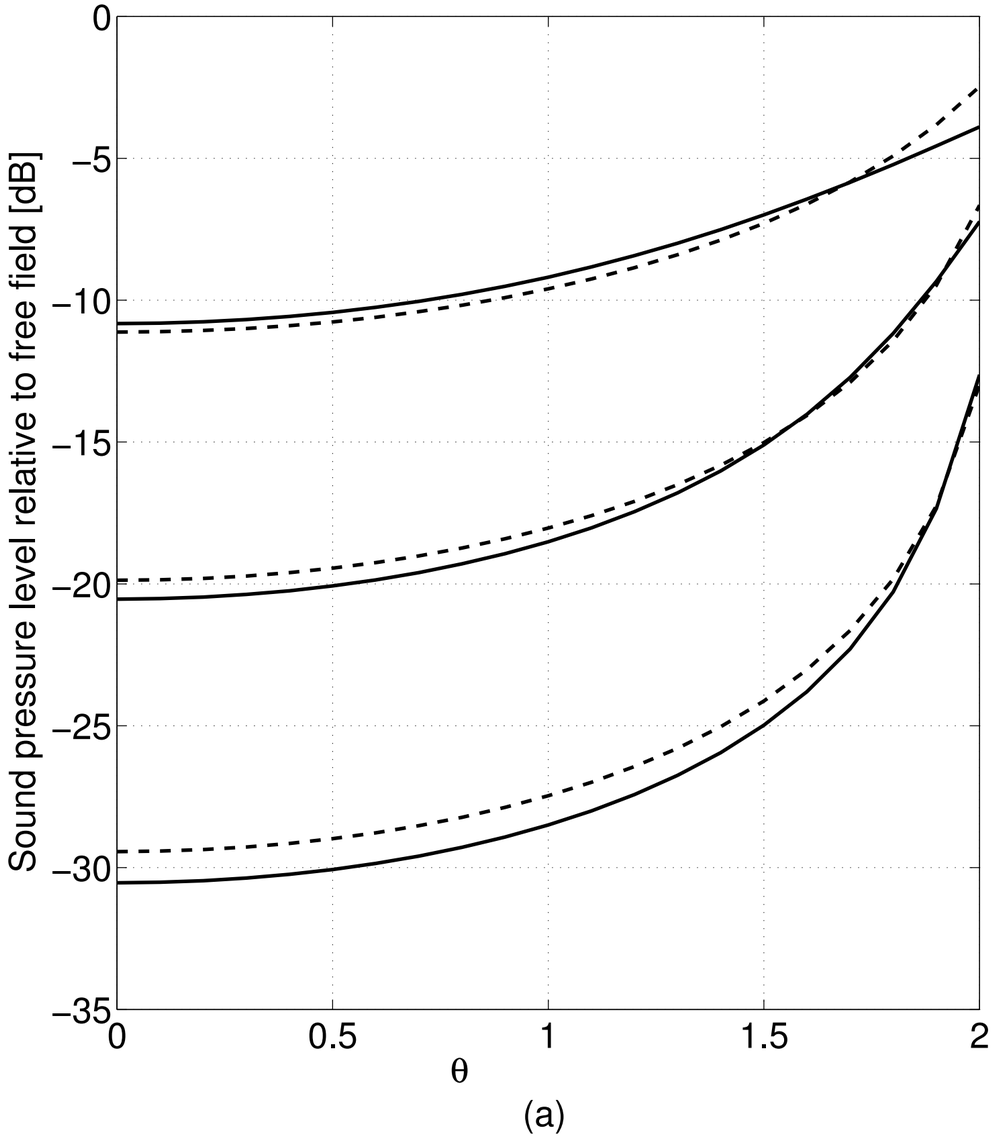
Sound pressure level relative to free field [dB]
0
−5
−10
−15
−20
−25
−30
−35
0
0.5
1
1.5
2
θ

(a)

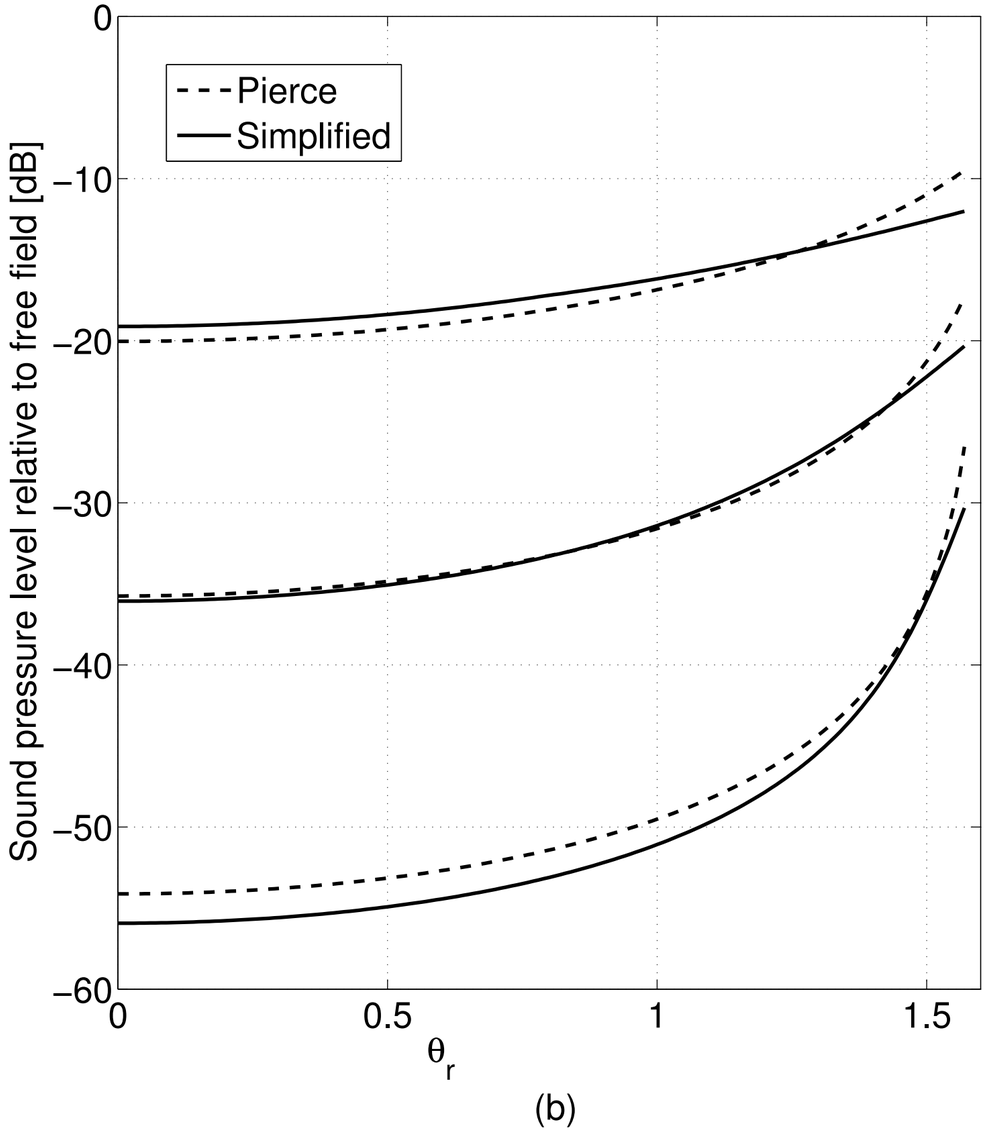
Pierce
Simplified
Sound pressure level relative to free field [dB]
0
−10
−20
−30
−40
−50
−60
0
0.5
1
1.5
θr

(b)

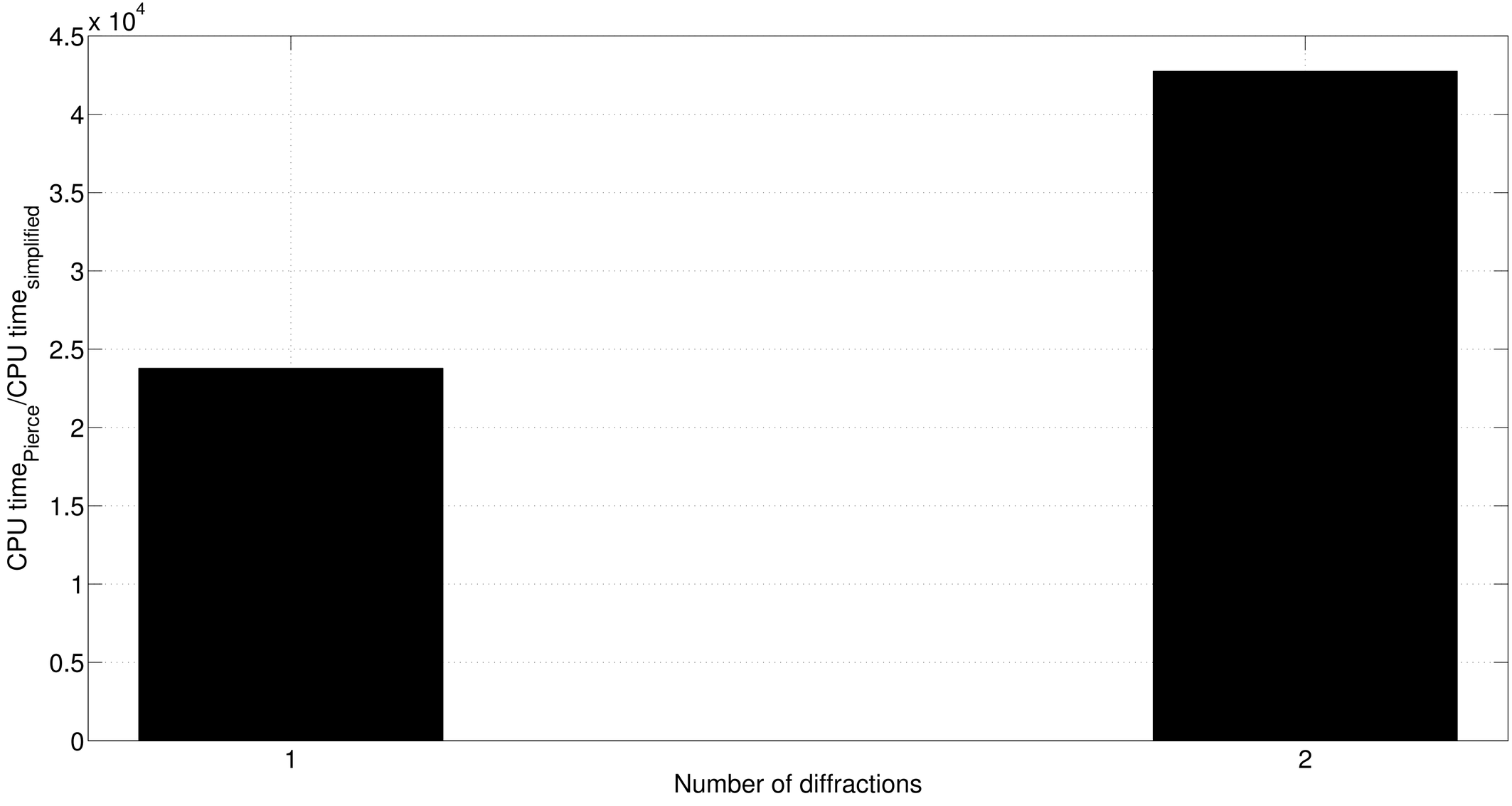
x 10^4
4.5
4
3.5
3
2.5
2
1.5
1
0.5
0
CPU time_Pierce/CPU time_simplified
1
2
Number of diffractions

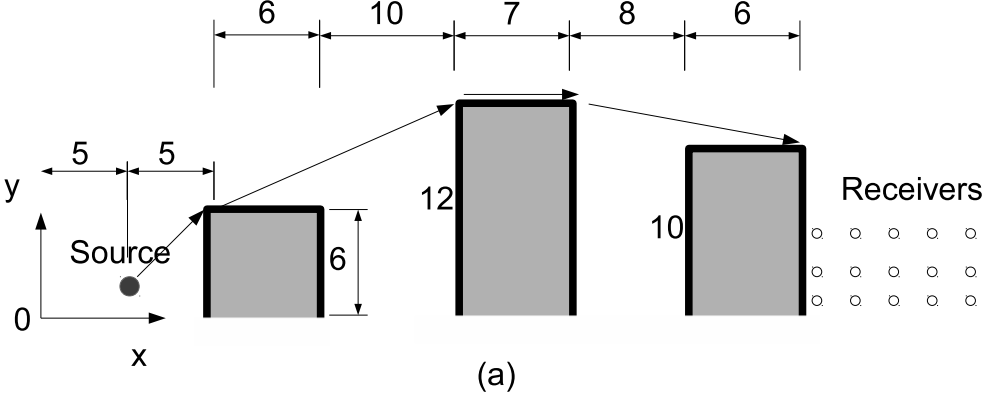
6
10
7
8
6
5
5
y
Source
6
12
10
Receivers
0
x

(a)

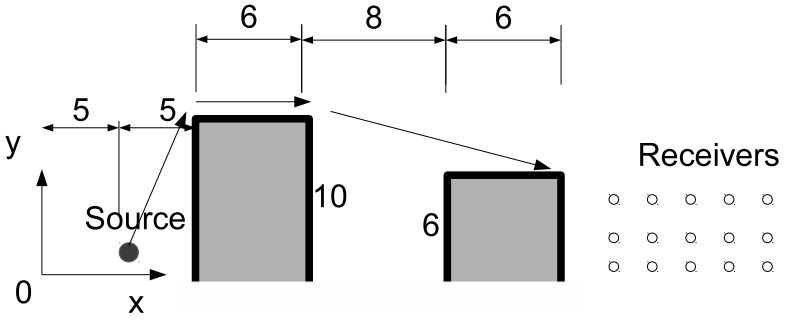
6
8
6
5
5
y
Source
10
6
Receivers
0
x

(b)

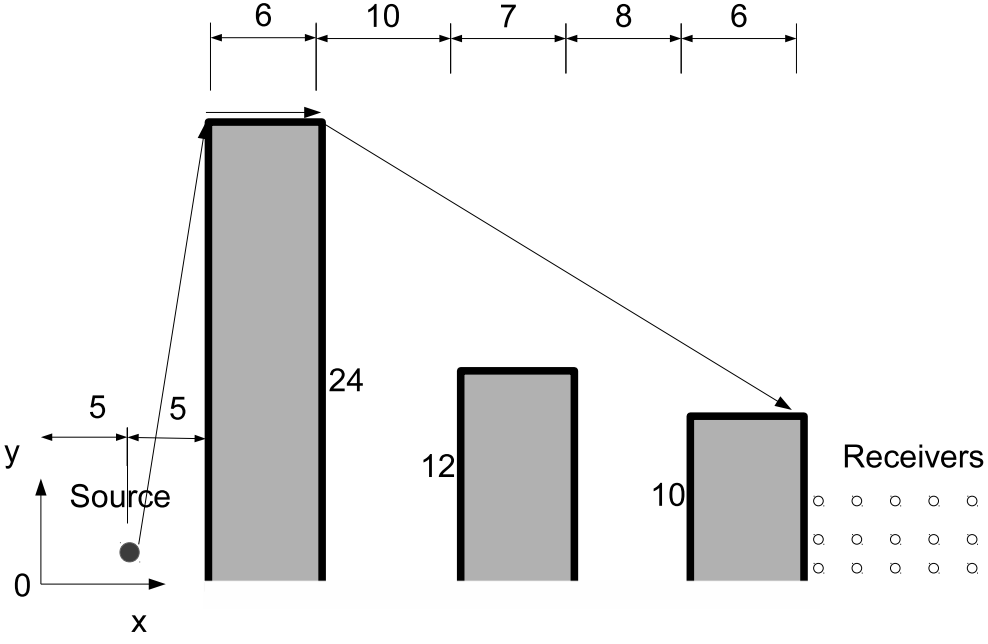
6
10
7
8
6
5
5
24
y
Source
12
10
Receivers
0
x

(c)

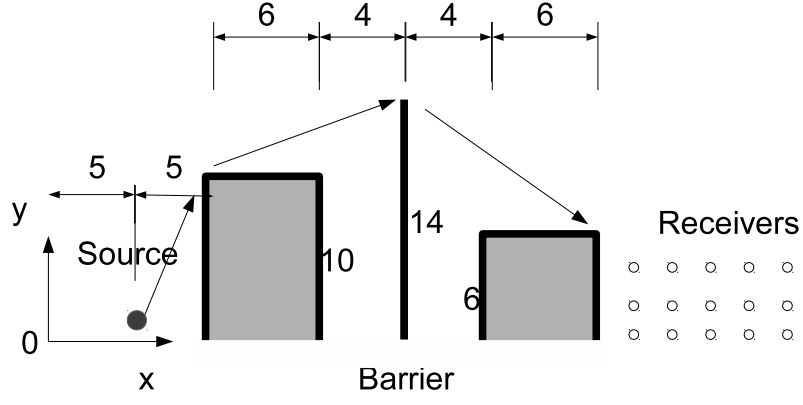
6
4
4
6
5
5
y
Source
10
14
6
Receivers
0
x
Barrier

(d)

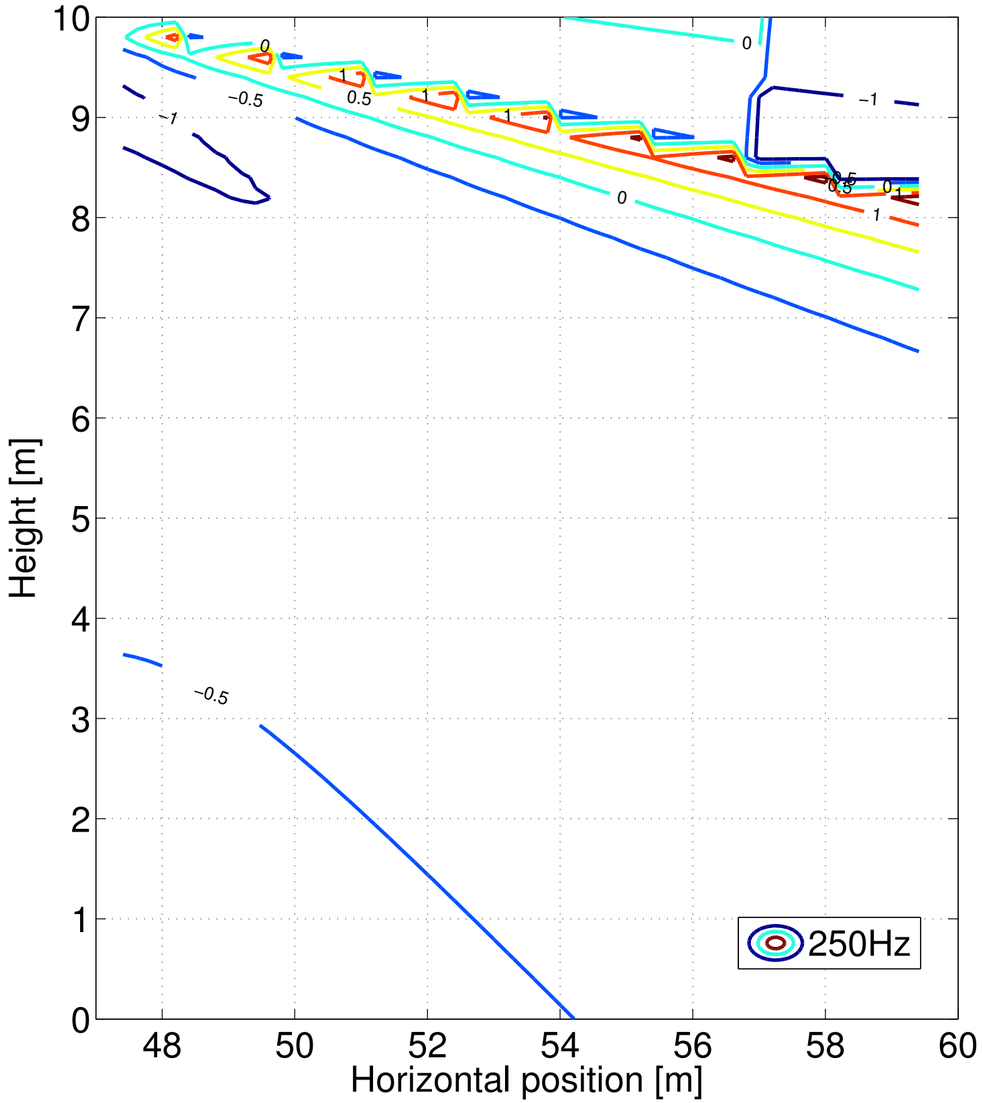
Height [m]
Horizontal position [m]
250Hz

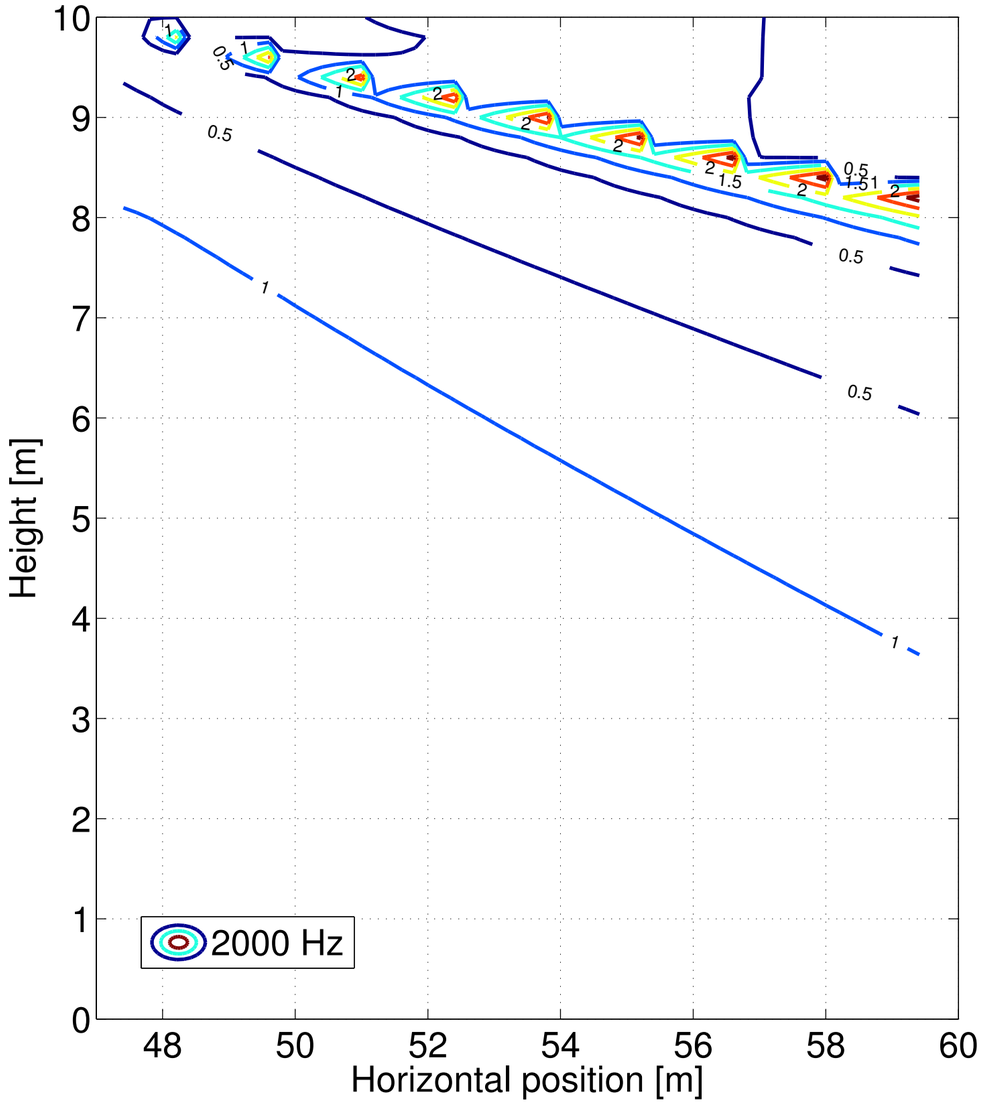
Height [m]
Horizontal position [m]
2000 Hz

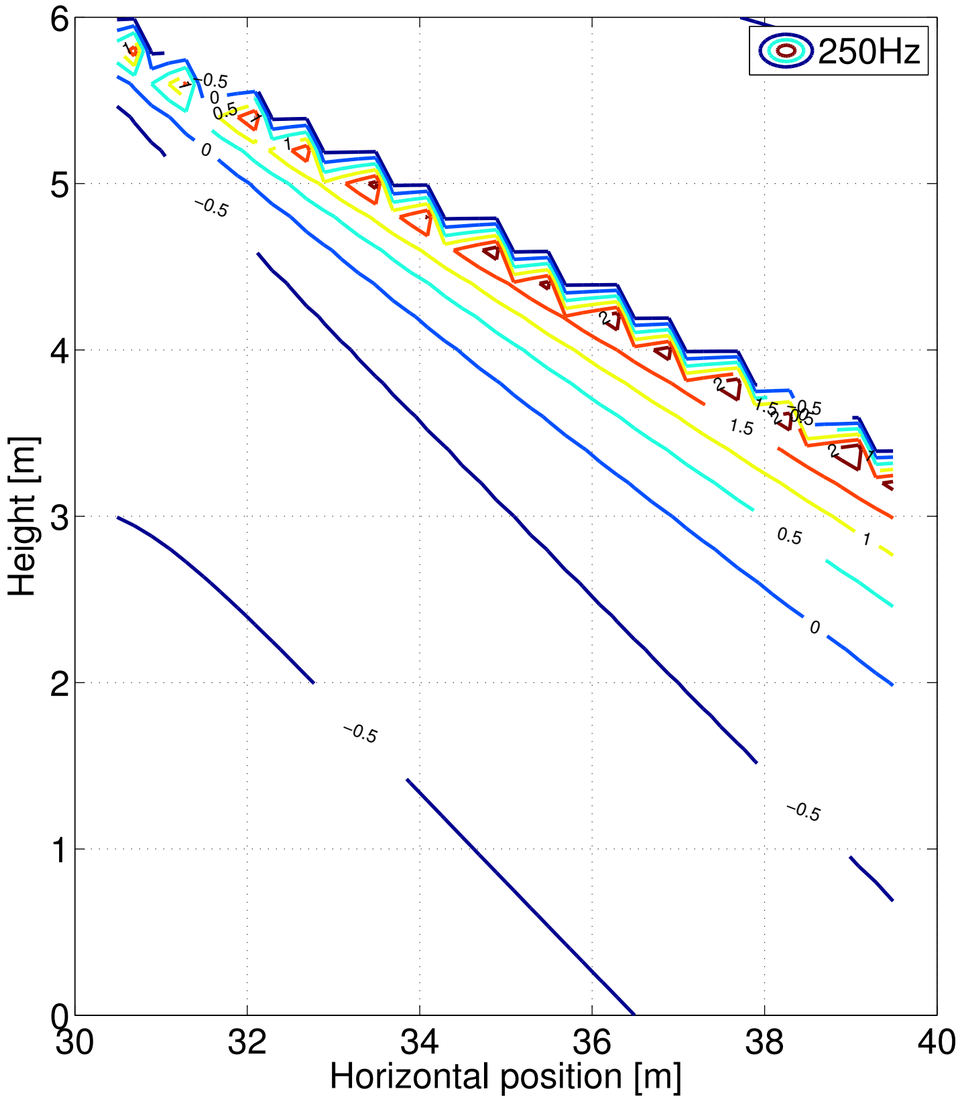
250Hz
Height [m]
Horizontal position [m]
0
1
2
3
4
5
6
30
32
34
36
38
40

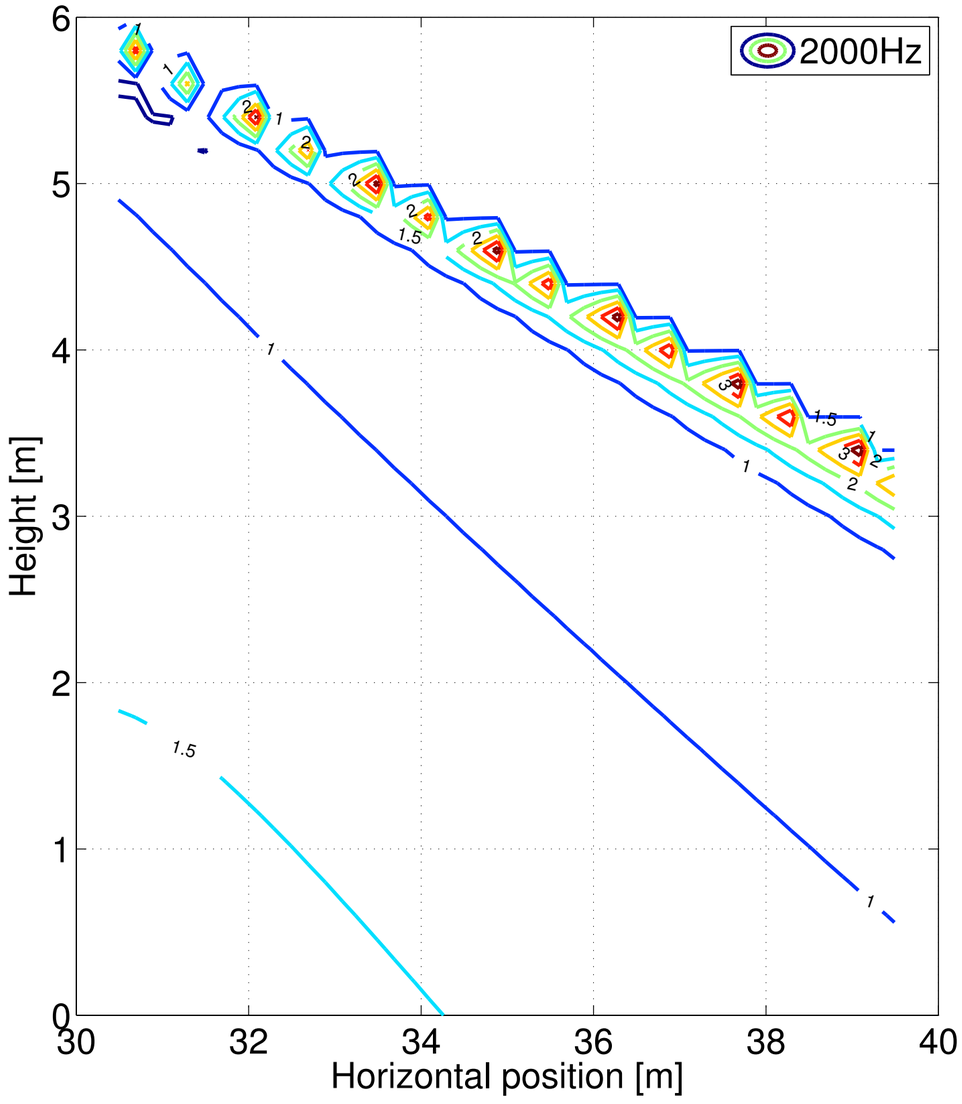
2000Hz
Height [m]
Horizontal position [m]
0
1
2
3
4
5
6
30
32
34
36
38
40

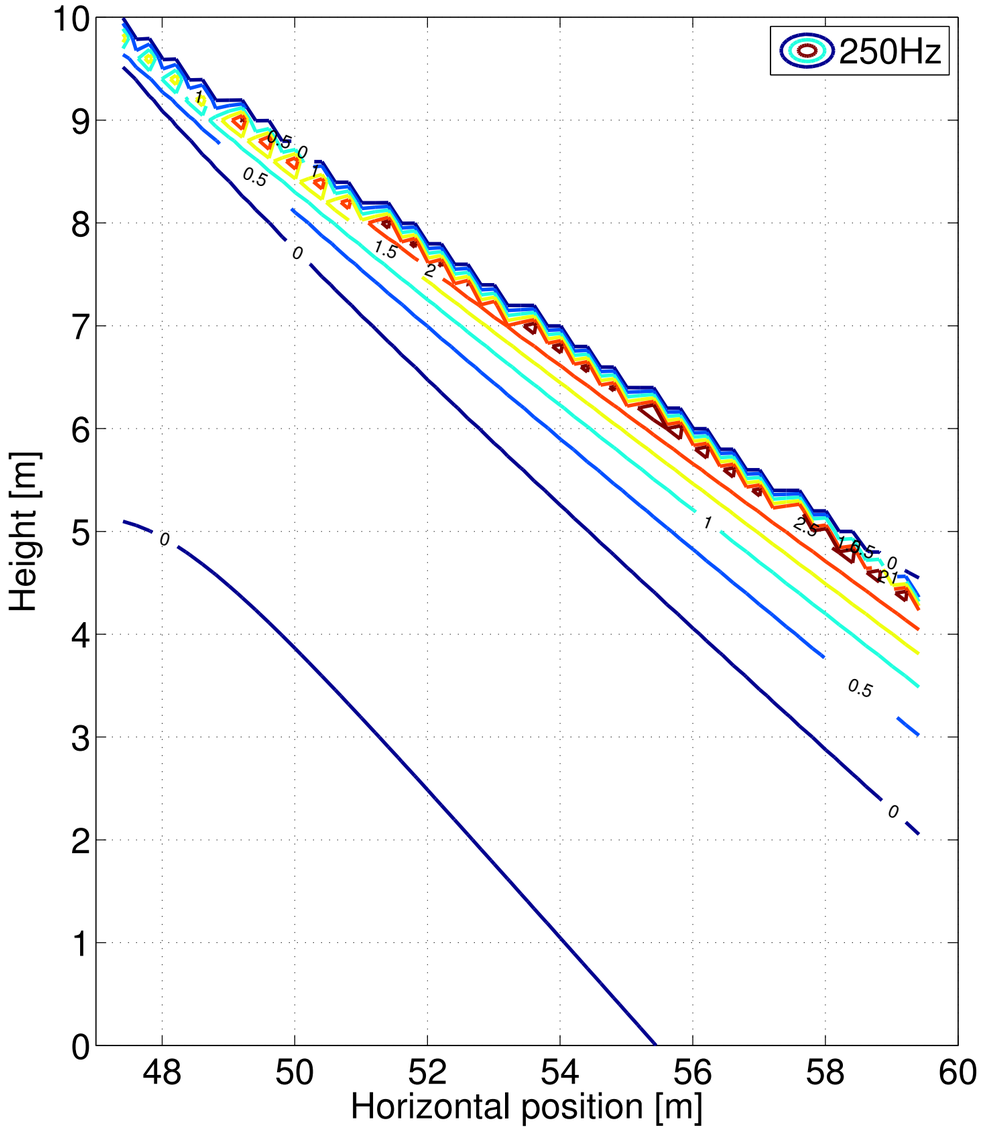
250Hz
Height [m]
Horizontal position [m]
0
1
2
3
4
5
6
7
8
9
10
48
50
52
54
56
58
60

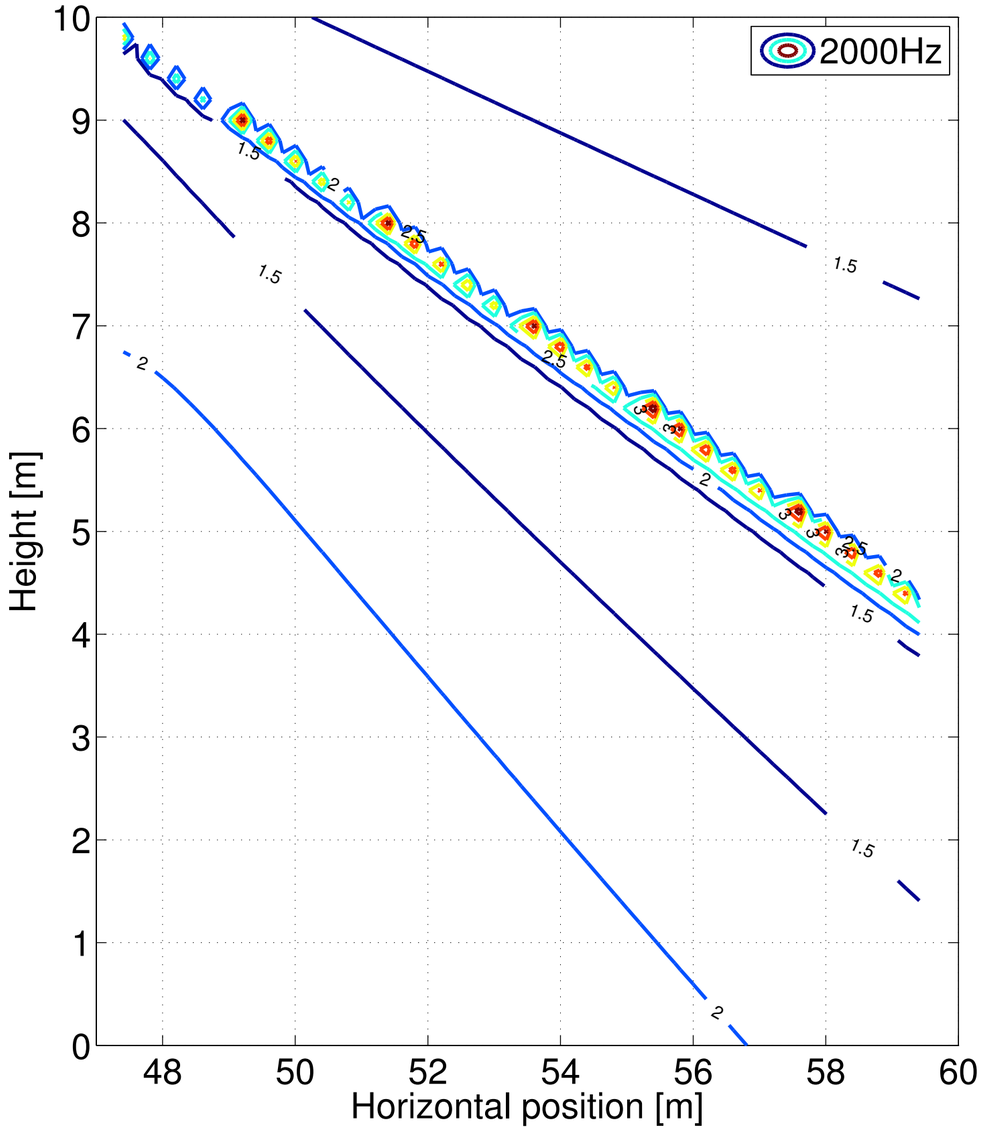
2000Hz
Height [m]
Horizontal position [m]
0
1
2
3
4
5
6
7
8
9
10
48
50
52
54
56
58
60

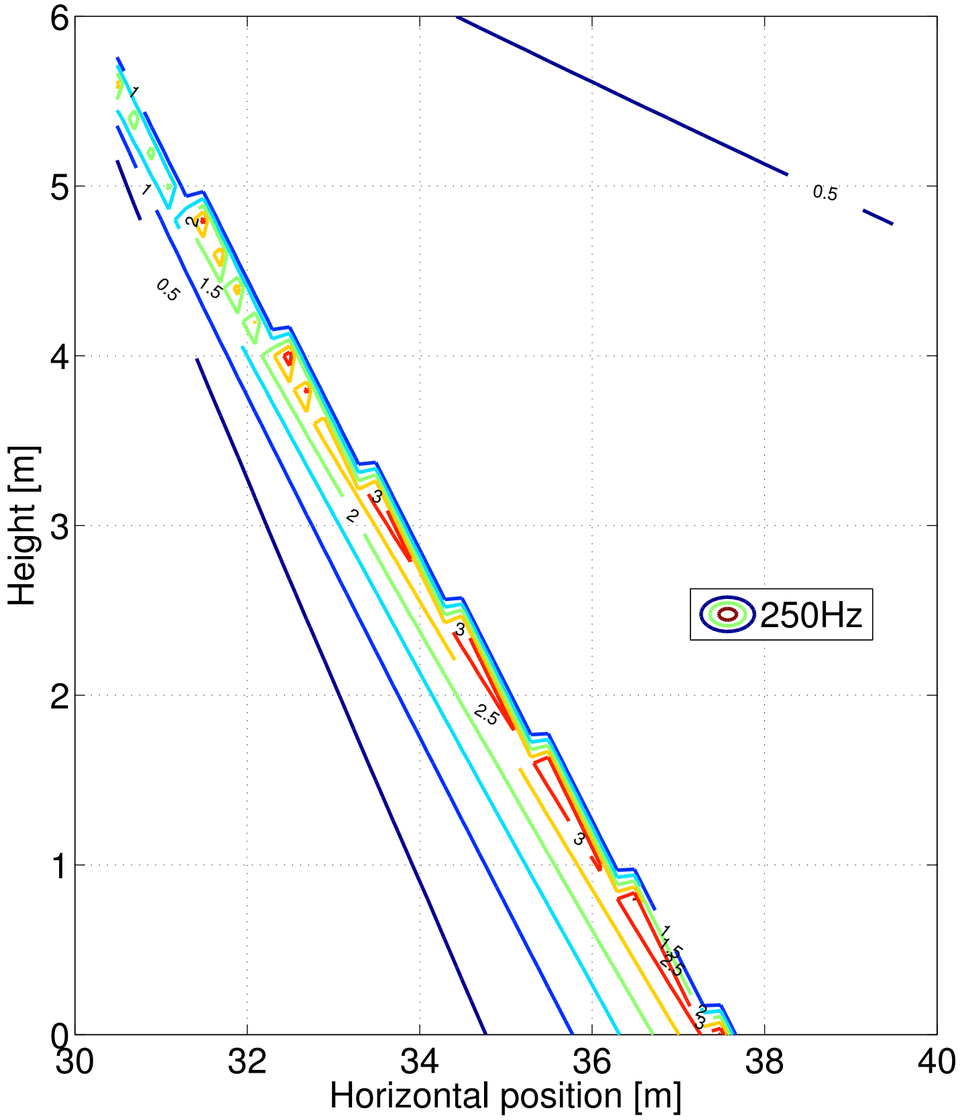
Height [m]
Horizontal position [m]
250Hz
0
1
2
3
4
5
6
30
32
34
36
38
40

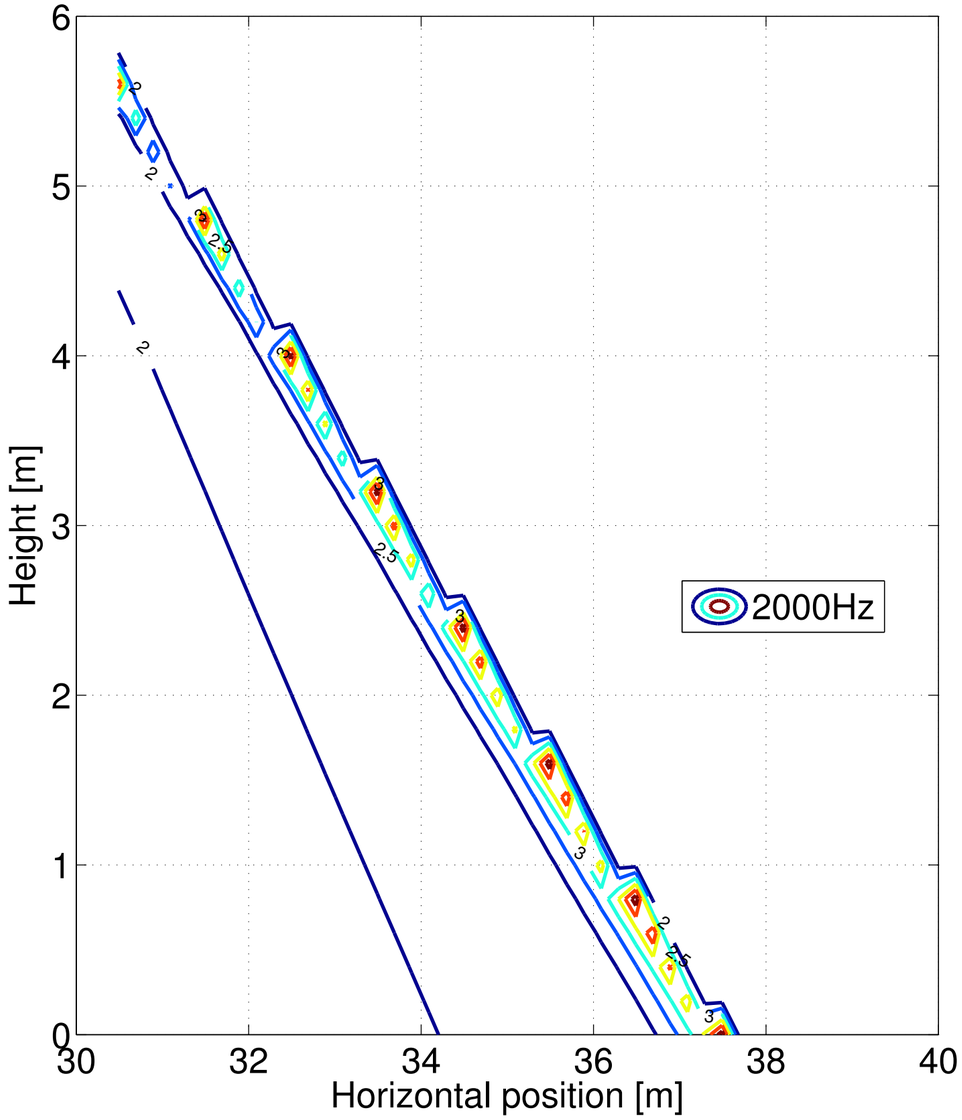
Height [m]
Horizontal position [m]
2000Hz
0
1
2
3
4
5
6
30
32
34
36
38
40

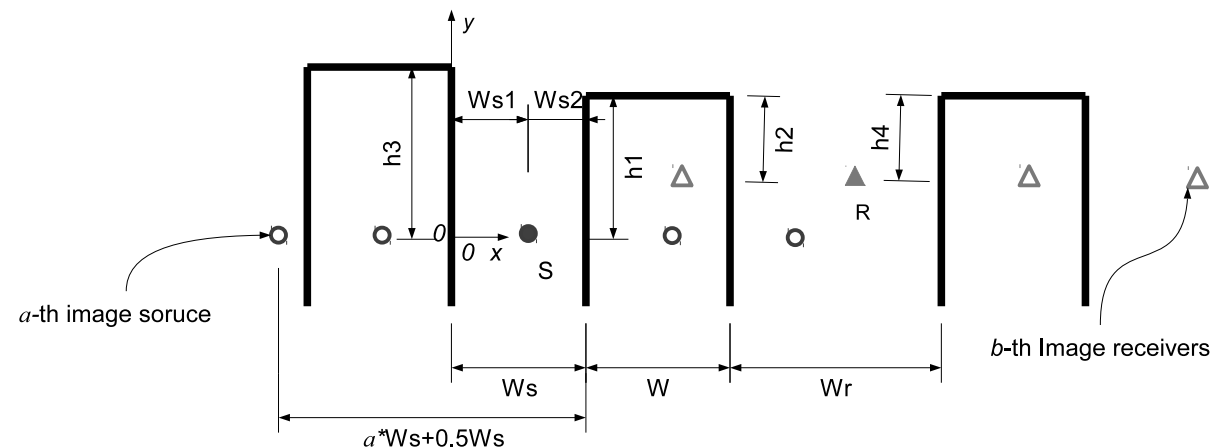
y
Ws1
Ws2
h3
h1
h2
h4
0
0
x
S
R
a-th image soruce
b-th Image receivers
Ws
W
Wr
a*Ws+0.5Ws

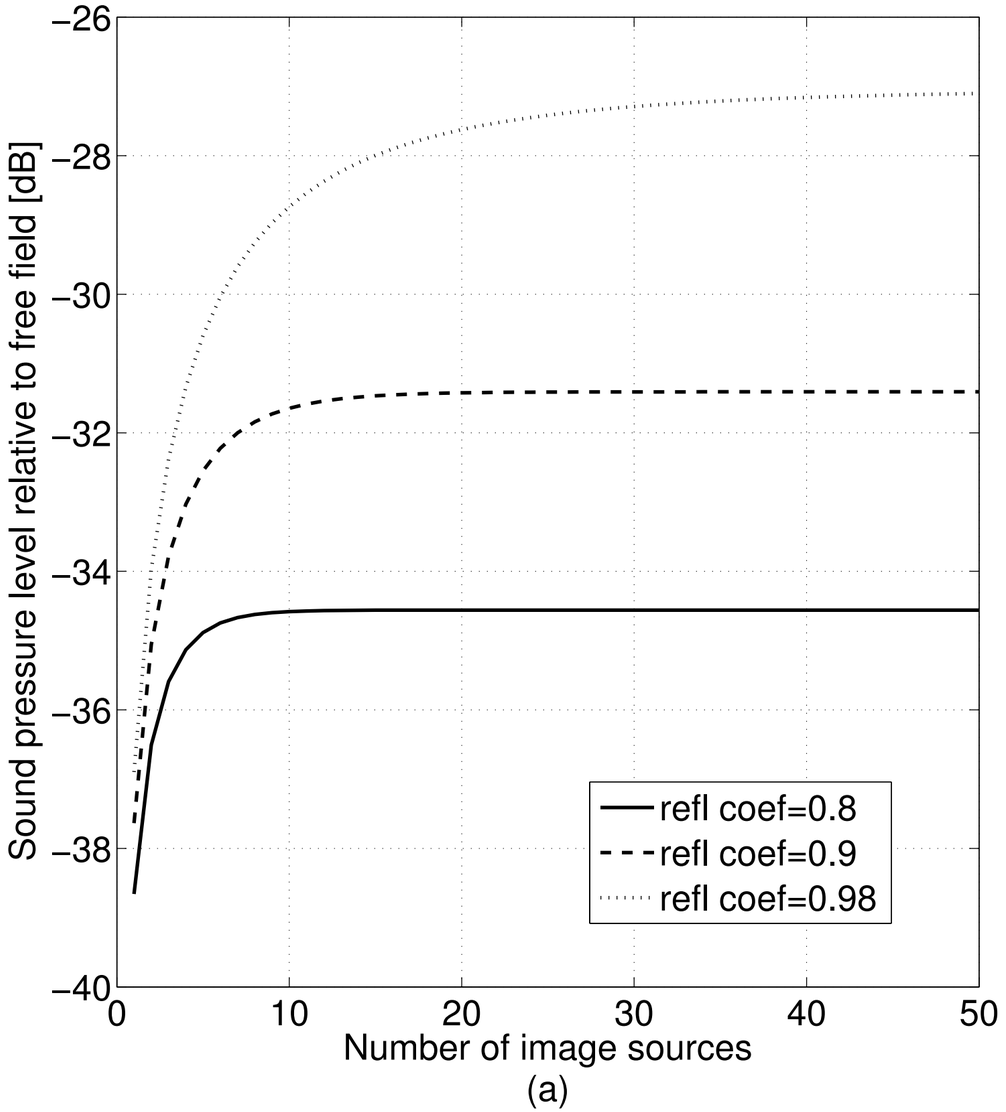
−26
−28
−30
−32
−34
−36
−38
−40
0
10
20
30
40
50
Sound pressure level relative to free field [dB]
Number of image sources
refl coef=0.8
refl coef=0.9
refl coef=0.98

(a)

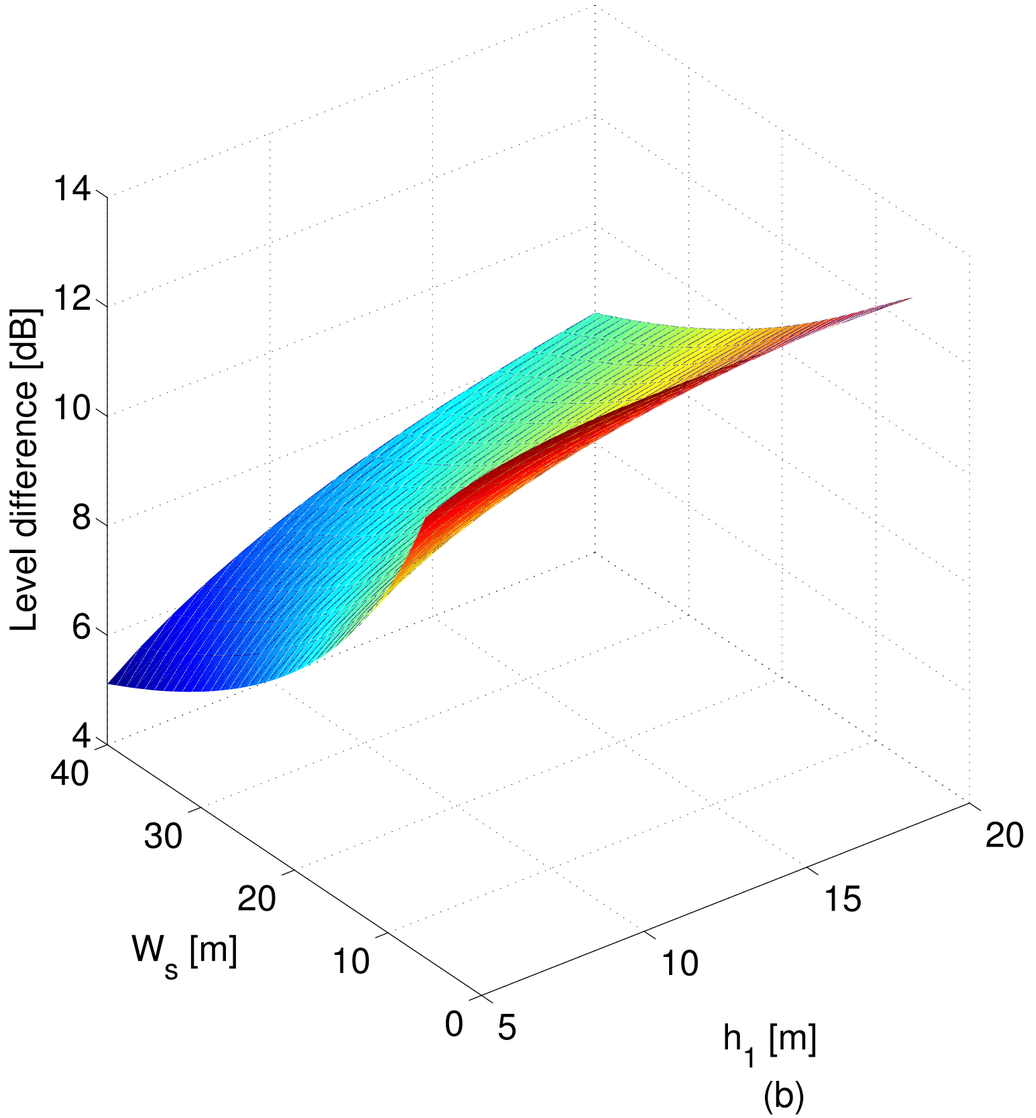
14
12
10
8
6
4
Level difference [dB]
40
30
20
10
0
$W_s$ [m]
5
10
15
20
$h_1$ [m]

(b)

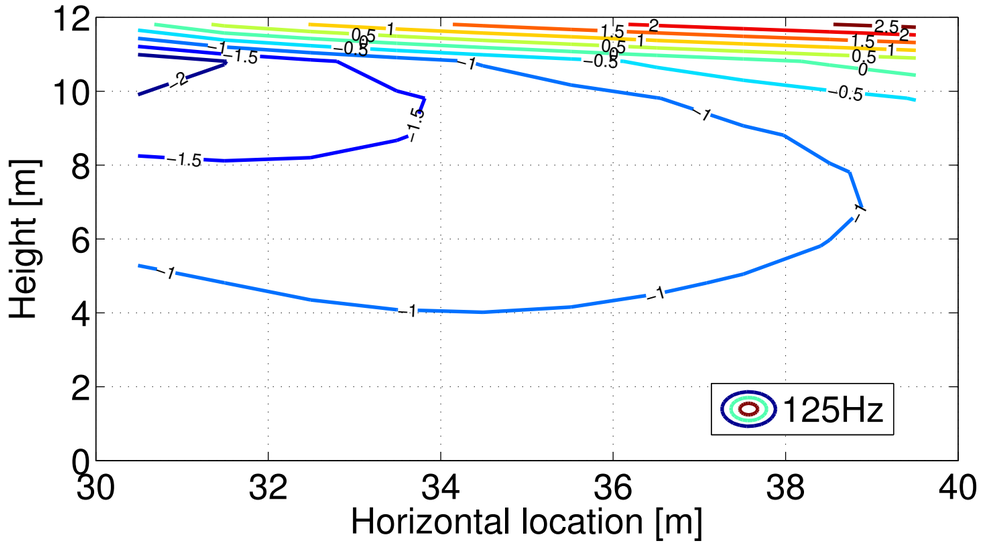
125Hz
Height [m]
Horizontal location [m]

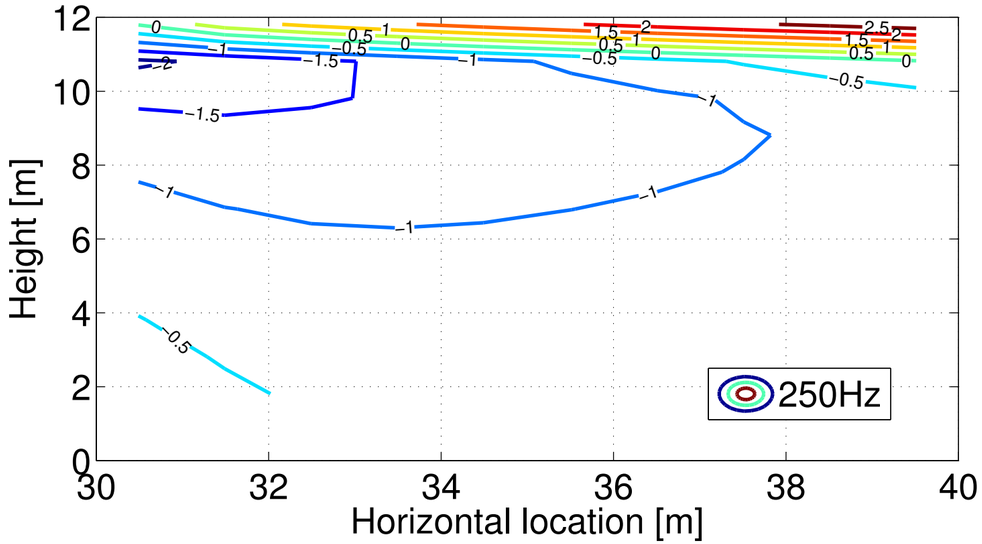
250Hz
Height [m]
Horizontal location [m]

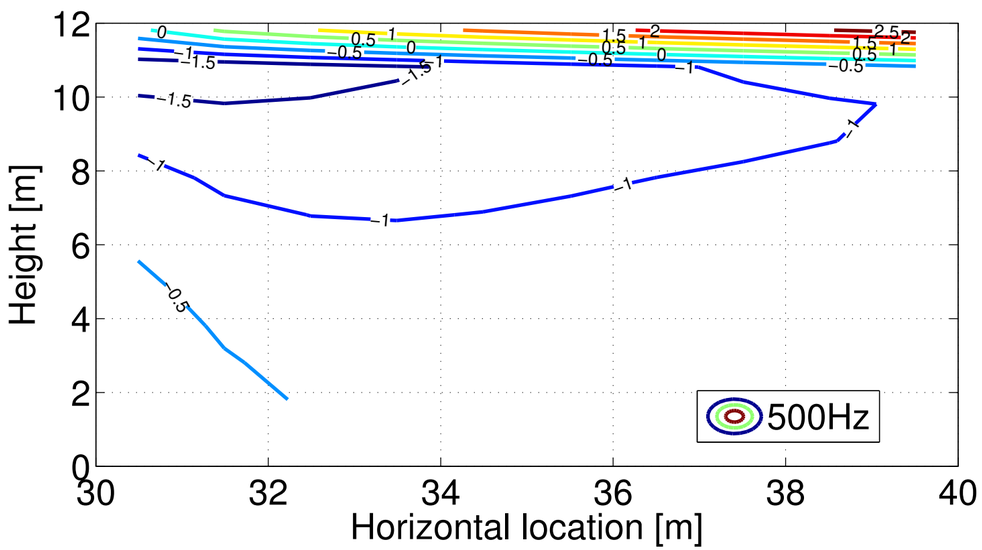
500Hz
Height [m]
Horizontal location [m]

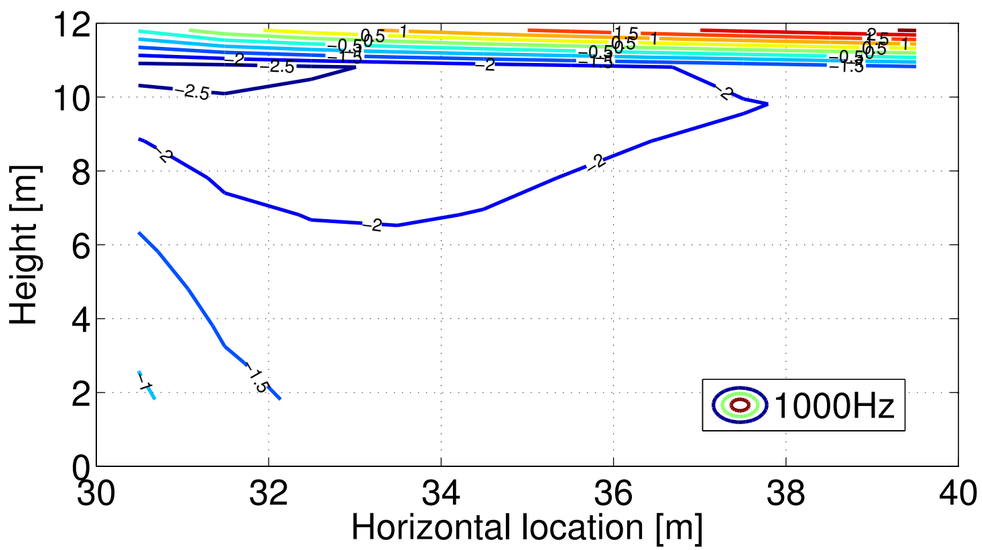
1000Hz
Height [m]
Horizontal location [m]

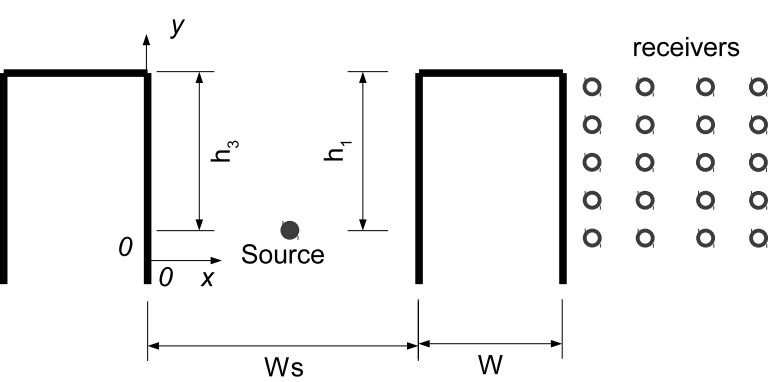
y
receivers
h3
h1
0
Source
0
x
Ws
W

(a)

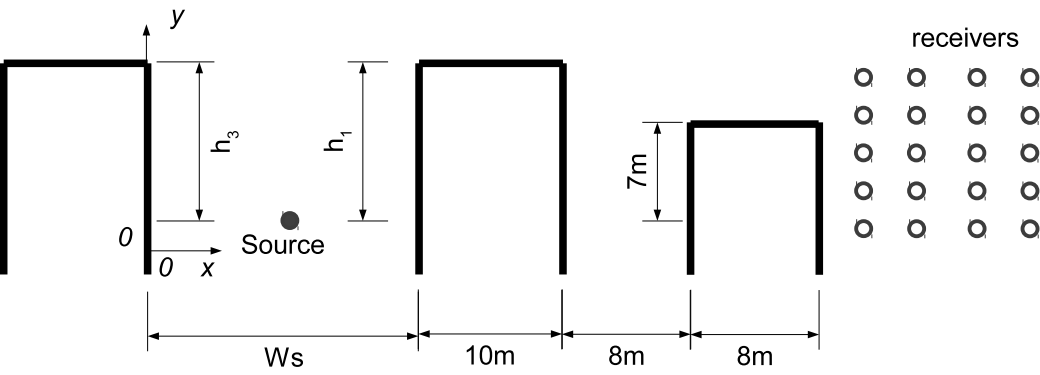
y
receivers
h3
h1
7m
0
Source
0
x
Ws
10m
8m
8m

(b)

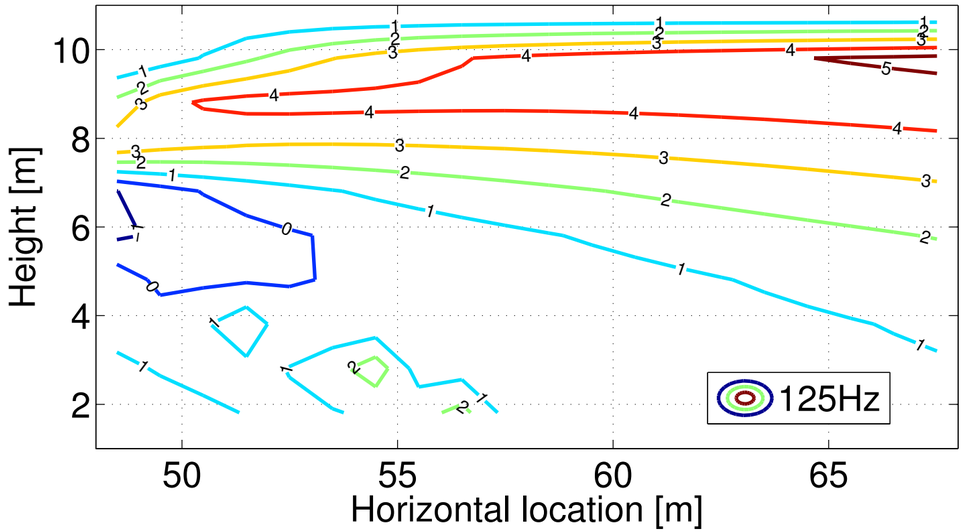
Height [m]
Horizontal location [m]
125Hz

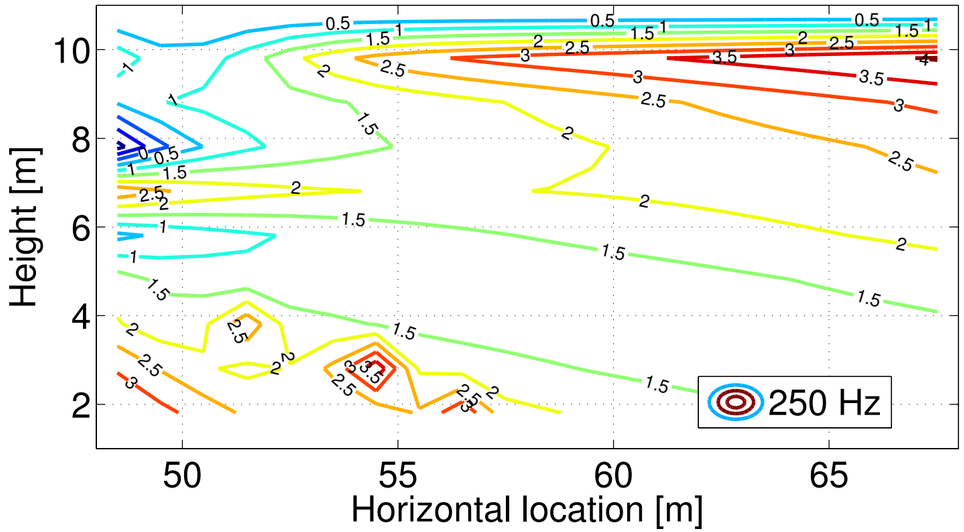
Height [m]
Horizontal location [m]
250 Hz

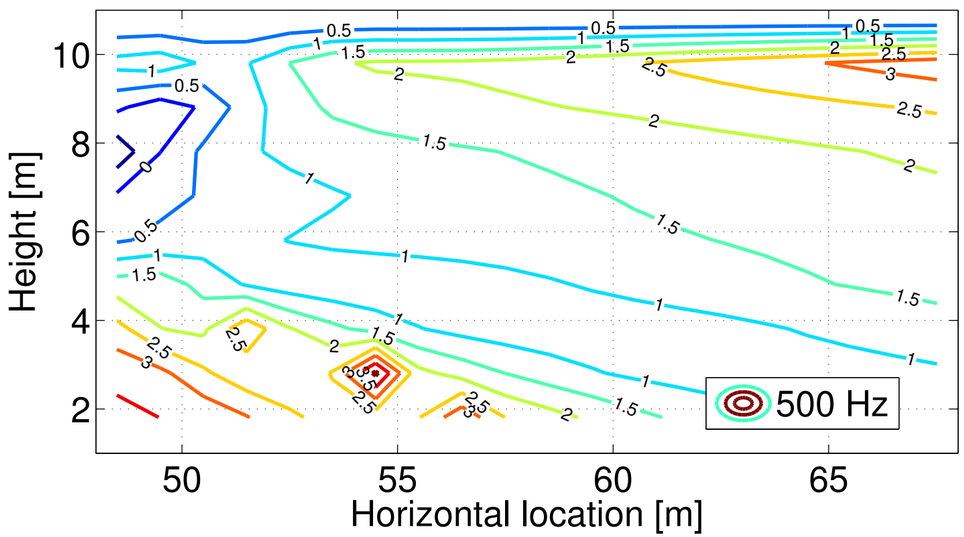
Height [m]
Horizontal location [m]
500 Hz

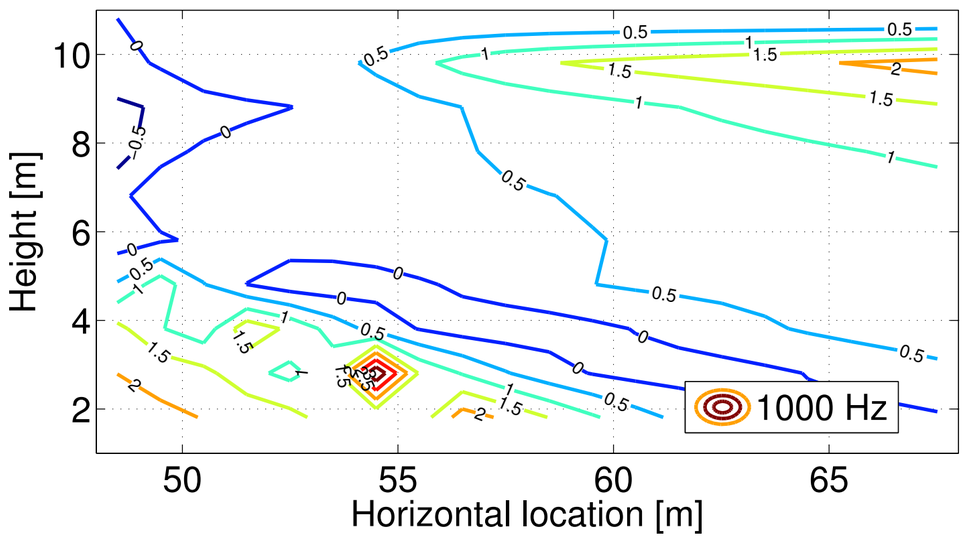
Height [m]
Horizontal location [m]
1000 Hz

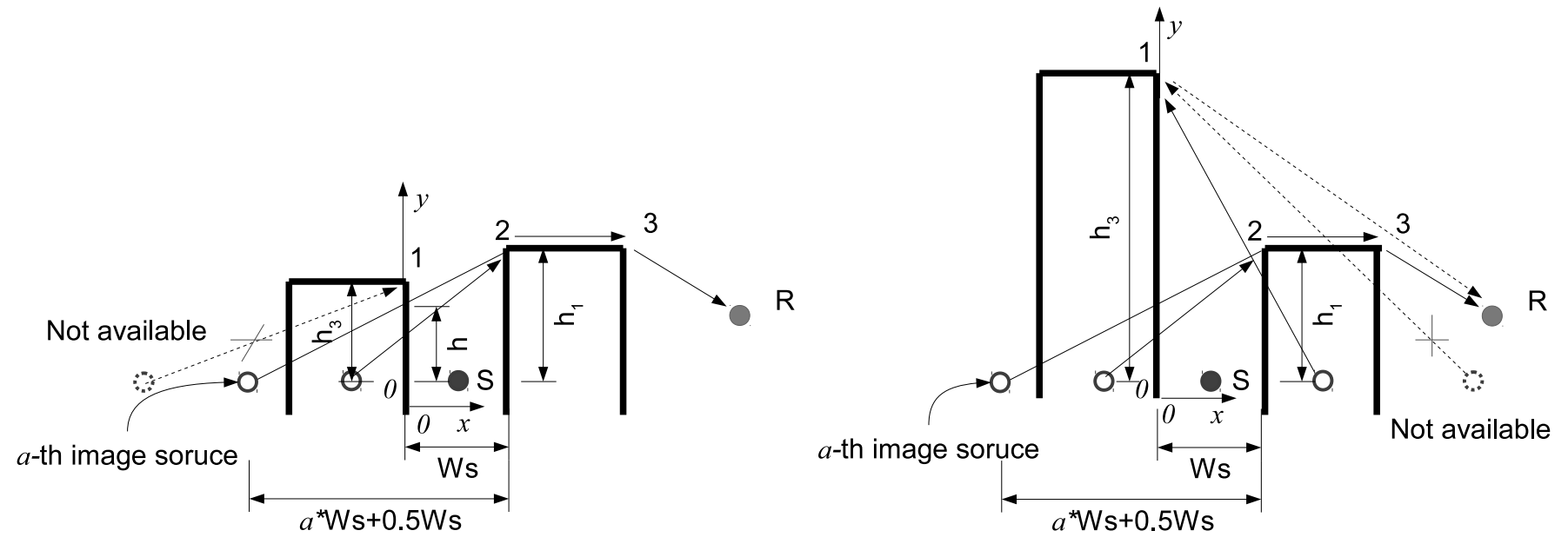
y
1
2
3
R
Not available
h3
h
h1
0
S
0
x
a-th image soruce
Ws
a*Ws+0.5Ws
(a)
y
1
2
3
R
h3
h1
0
S
0
x
a-th image soruce
Not available
Ws
a*Ws+0.5Ws
(b)

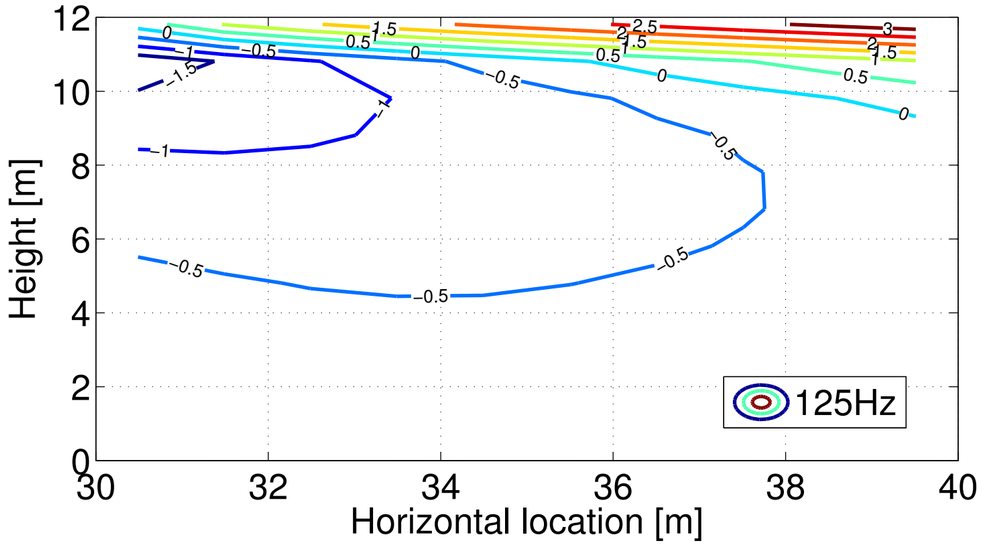
Height [m]
Horizontal location [m]
125Hz

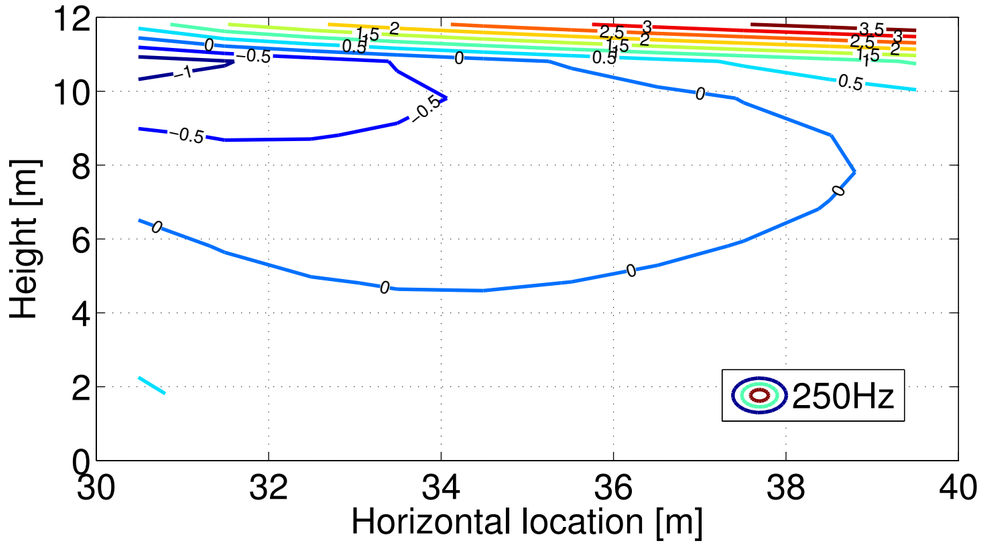
Height [m]
Horizontal location [m]
250Hz

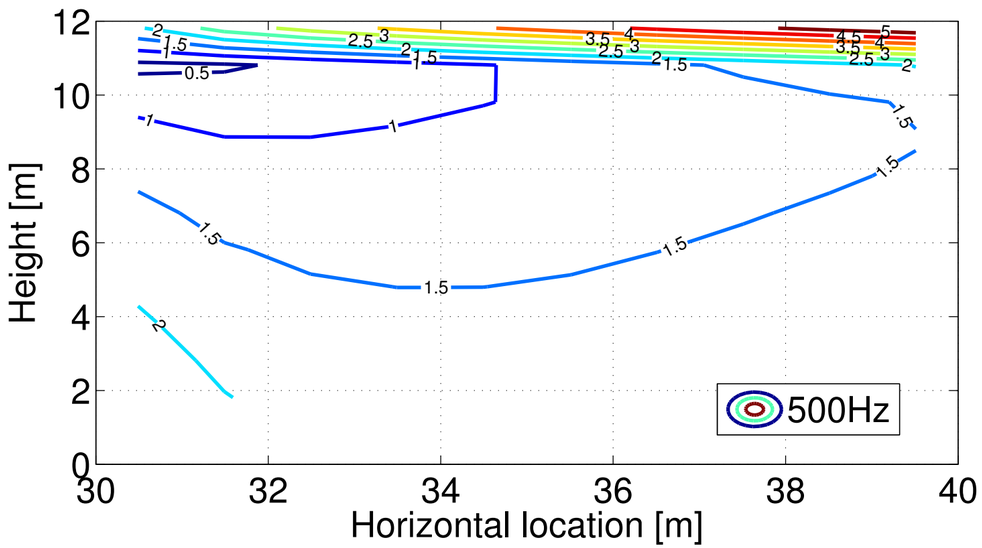
Height [m]
Horizontal location [m]
500Hz

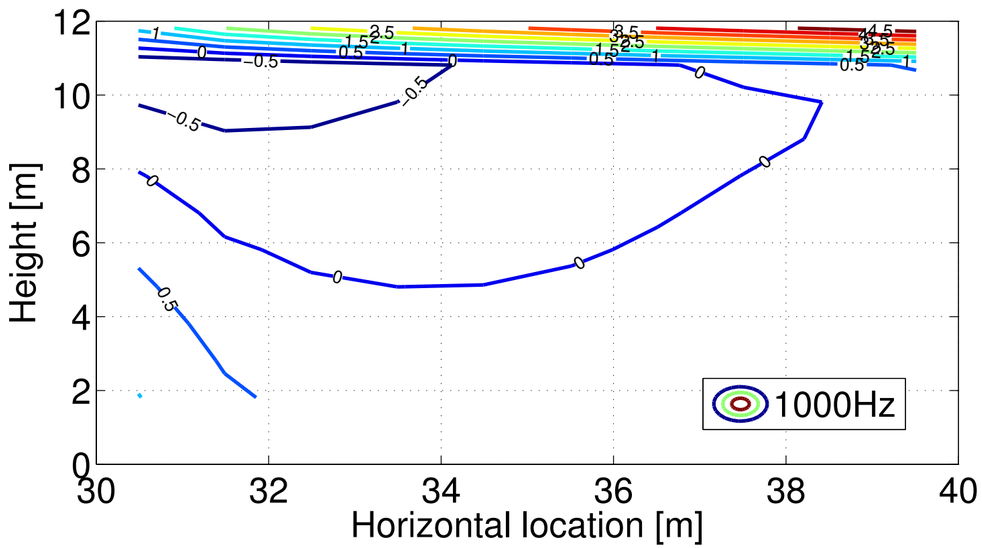
Height [m]
Horizontal location [m]
1000Hz

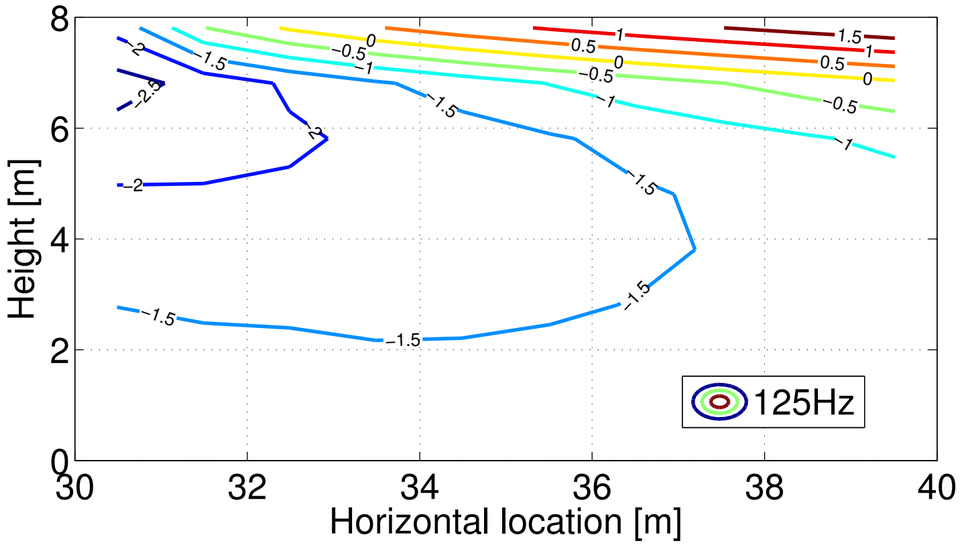
Height [m]
Horizontal location [m]
125Hz

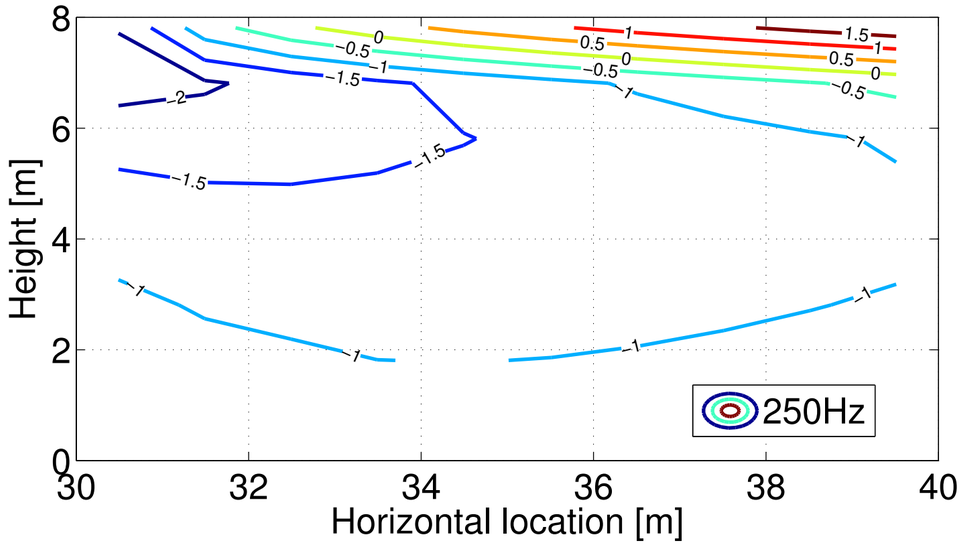
Height [m]
Horizontal location [m]
250Hz

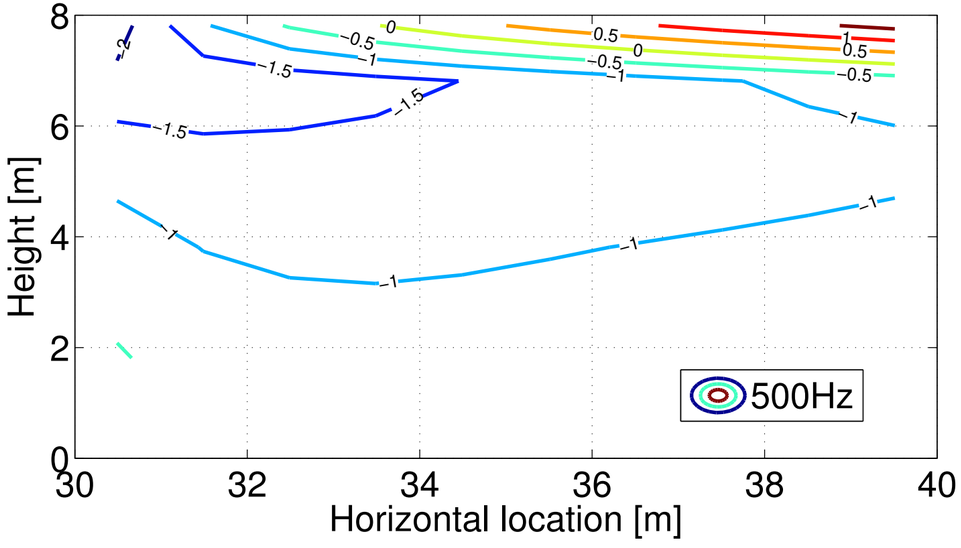
Height [m]
Horizontal location [m]
500Hz

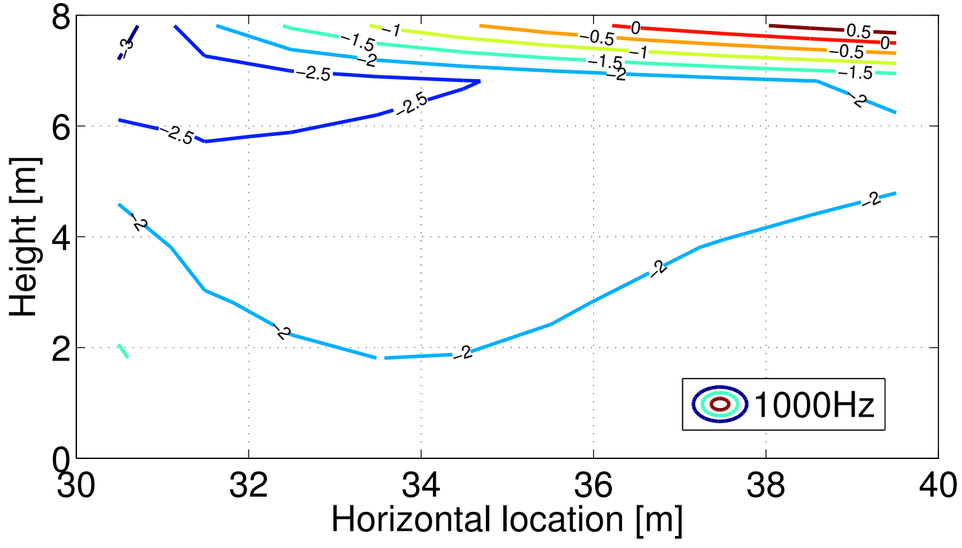
Height [m]
Horizontal location [m]
1000Hz

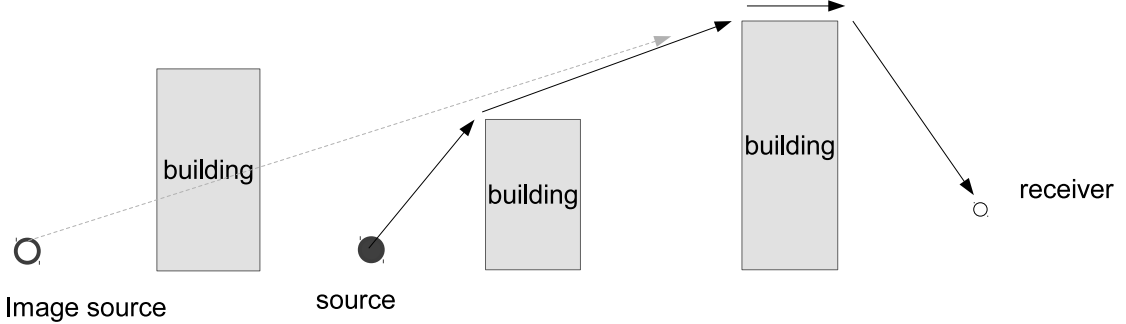
building
building
building
receiver
Image source
source

(a)

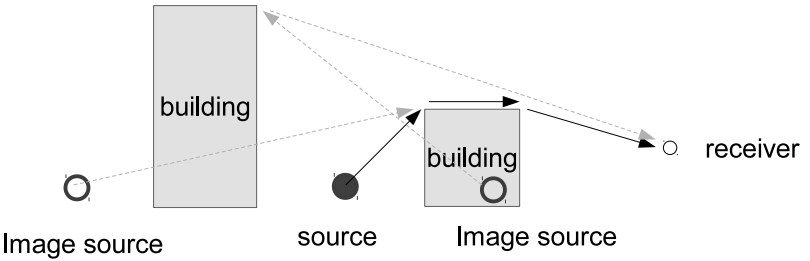
building
building
receiver
Image source
source
Image source

(b)

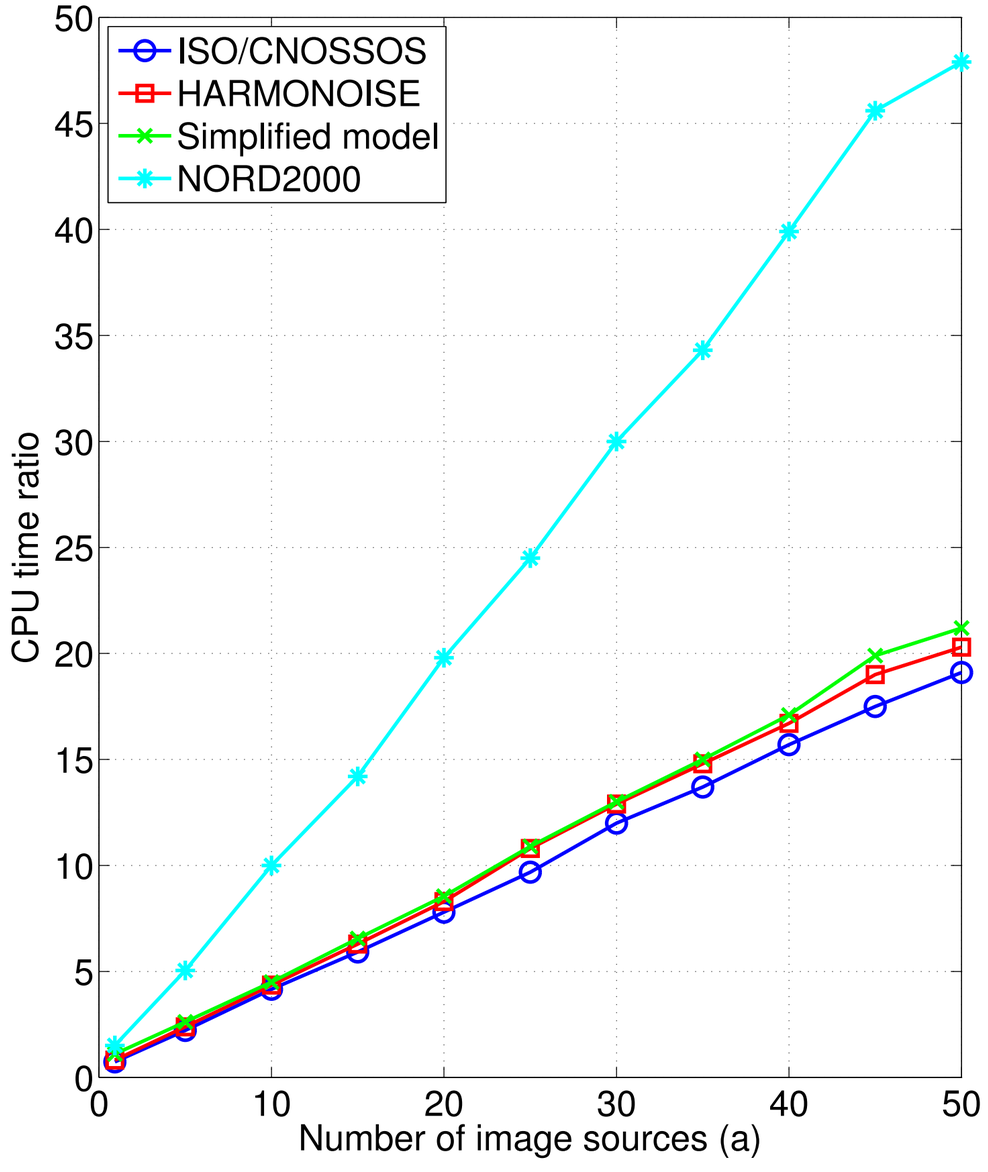
ISO/CNOSSOS
HARMONOISE
Simplified model
NORD2000
CPU time ratio
Number of image sources (a)
0
5
10
15
20
25
30
35
40
45
50
0
10
20
30
40
50

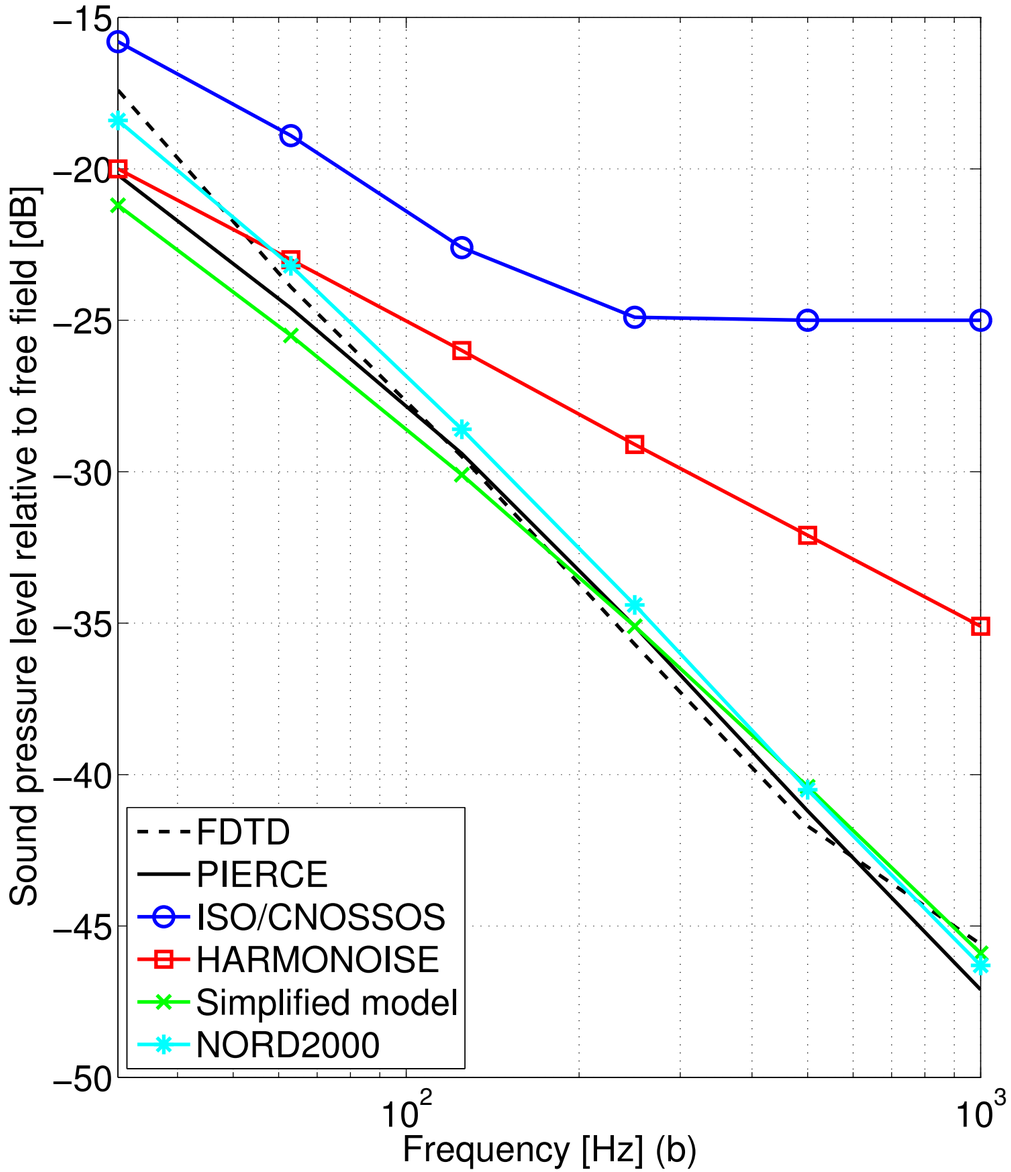
FDTD
PIERCE
ISO/CNOSSOS
HARMONOISE
Simplified model
NORD2000
Sound pressure level relative to free field [dB]
Frequency [Hz] (b)
−15
−20
−25
−30
−35
−40
−45
−50
$10^2$
$10^3$